De novo evolution of macroscopic multicellularity

G. Ozan Bozdag [1,†,*], Seyed Alireza Zamani-Dahaj[2,3,*], Thomas C. Day[3], Penelope C. Kahn[1,4], Anthony J. Burnetti[1], Dung T. Lac[1], Kai Tong[1,2], Peter L. Conlin[1], Aishwarya H. Balwani[5], Eva L. Dyer[5], Peter J. Yunker[2,†] and William C. Ratcliff[1,†]

[1]School of Biological Sciences, Georgia Institute of Technology, Atlanta, GA, USA

[2]Interdisciplinary Graduate Program in Quantitative Biosciences, Georgia Institute of Technology, Atlanta, GA, USA

[3]School of Physics, Georgia Institute of Technology, Atlanta, GA, USA

[4]Department of Zoology, University of British Columbia, Vancouver, British Columbia, Canada

[5]School of Electrical & Computer Engineering, Georgia Institute of Technology, Atlanta, GA, USA

[*]These authors contributed equally to this work.

[†]Corresponding authors: ozan.bozdag@gmail.com, ratcliff@gatech.edu, peter.yunker@gatech.edu

Abstract

While early multicellular lineages necessarily started out as relatively simple groups of cells, little is known about how they became Darwinian entities capable of open-ended multicellular adaptation[1,2]. To explore this, we initiated the Multicellularity Long Term Evolution Experiment (MuLTEE), selecting for larger group size in the snowflake yeast (*Saccharomyces cerevisiae*) model system. Given the historical importance of oxygen limitation[3], our ongoing experiment consists of three metabolic treatments[4]: anaerobic, obligately aerobic, and mixotrophic yeast. After 600 rounds of selection, snowflake yeast in the anaerobic treatment evolved to be macroscopic, becoming ~$2 \cdot 10^4$ times larger (~mm scale) and ~10^4-fold more biophysically tough, while retaining a clonal multicellular life cycle. They accomplished this through sustained biophysical adaptation, evolving increasingly elongate cells that initially reduced the strain of cellular packing, then facilitated branch entanglements that enabled groups of cells to stay together even after many cellular bonds fracture. In contrast, snowflake yeast competing for low oxygen remained microscopic, evolving to be just ~6-fold larger, underscoring the critical role of oxygen levels in the evolution of multicellular size. Taken together, this work provides unique insight into an ongoing evolutionary transition in individuality, showing how simple groups of cells overcome fundamental biophysical limitations via gradual, yet sustained, multicellular adaptation.

Introduction

Organismal size plays a fundamental role in the evolution of multicellularity. The evolution of larger size allows organisms to gain protection from the external environment[5] and explore novel niches[6], while creating opportunities for the evolution of cellular differentiation[7-11]. Increases in organismal size have also been hypothesized to play a key role in the evolution of trade-off breaking multicellular innovations, as large size creates an evolutionary incentive to solve challenges of nutrient and oxygen transportation that are otherwise inescapable consequences of diffusion limitations[12,13]. However, little is known about how nascent multicellular organisms, consisting of small groups of undifferentiated cells, evolve to form biomechanically tough, macroscopic multicellular bodies, and whether selection for size itself can drive sustained multicellular adaptation[3].

The evolution of macroscopic size presents a fundamental challenge to nascent multicellular organisms, requiring the evolution of biophysical solutions to evolutionarily-novel stresses that act over previously-unseen multicellular size scales[14-18]. While prior work with yeast and algae have shown that novel multicellularity is relatively easy to evolve *in vitro,* these organisms remain microscopic, typically growing to a maximum size of tens to hundreds of cells[19-23]. Extant macroscopic multicellular organisms have solved the above challenges through developmental innovation, evolving mechanisms that either reduce the accumulation of biophysical strain or increase multicellular toughness[24-26]. However, in nascent multicellular organisms that have not yet evolved coordinated morphogenesis, we do not know how, or even whether, simple groups of cells can evolve the increased biophysical toughness required for the evolution of macroscopic size.

Here we examine the interplay between biological, biophysical, and environmental drivers of macroscopic multicellularity using long-term experimental evolution. We subject snowflake yeast[21], a model of undifferentiated multicellularity, to 600 rounds (~3,000 generations) of daily selection for increased size. Furthermore, because oxygen is thought to have played a key role in the evolution of macroscopic multicellularity, we evolved snowflake yeast with either anaerobic, mixotrophic, or obligately aerobic metabolism. All five of our replicate anaerobic populations evolved macroscopic size, while all aerobic and mixotrophic populations remained microscopic throughout the experiment, supporting the hypothesis that growth under low concentrations of oxygen constraint the evolution of large multicellular size[4]. Macroscopic size convergently evolved through two key changes in all five replicate populations. First, snowflake yeast increased the length of their constituent cells, which delays organismal fracture caused by packing-induced strain[18]. Next, they evolved to entangle branches of connected cells such that breaking a single cell-cell bond no longer causes multicellular fracture, evolving to become $\sim 2 \cdot 10^5$ times larger, forming millimeter-scale groups of clonal cells. Together these adaptations increased the toughness of individual clusters by more than 10^4-fold, transforming the initial snowflake yeast ancestor, which was weaker than gelatin, to an organism with the strength and toughness of wood. Fitness assays, sequencing, and synthetic strain constructions reveal that macroscopic multicellularity evolved via selection acting on group size, an emergent multicellular trait of mutations directly affecting cellular morphology.

Results

In 2018 we initiated the Multicellularity Long Term Evolution Experiment (MuLTEE), named after the pioneering Long Term Evolution Experiment with *E. coli* initiated by Rich Lenski[27]. This central goal of this project, which we intend to run over decadal time scales, is to observe open-

89 ended multicellular adaptation in a nascent multicellular organism. We began the MuLTEE by
90 engineering a unicellular isolate of *S. cerevisiae* strain Y55 to grow with the snowflake phenotype
91 by deleting the *ACE2* open reading frame, ensuring that each replicate population had the same
92 initial mechanism of group formation[28]. To examine the effect of oxygen on the evolution of size,
93 we initiated three treatments in an otherwise isogenic ancestor: anaerobic growth (generated by
94 selecting for a spontaneous petite mutant incapable of respiration), mixotrophy (cultured with
95 glucose as the primary carbon source), and obligately aerobic growth (cultured with glycerol as
96 the primary carbon source)[4]. We refer to the five replicate populations of anaerobic, mixotrophic,
97 and obligately aerobic populations as PA, PM, and PO 1-5, respectively. We maintained strong
98 directional selection favoring larger cluster size throughout the experiment by selecting for
99 increasingly rapid sedimentation prior to transfer to fresh media (see Methods for details). We
100 evolved these 15 populations over 600 rounds of growth and settling selection (~3,000 generations,
101 Fig. 1A).

102 All five populations of anaerobic snowflake yeast evolved macroscopic size, with
103 individual clusters visible to the naked eye (Fig. 1B-D, Supplementary Movie 1). In contrast,
104 snowflake yeast capable of metabolizing oxygen remained microscopic (Fig. 1A & Extended Data
105 Fig. 1), a result consistent with recent work showing that competition for scarce oxygen imposes
106 a powerful constraint on the evolution of large multicellular size[4]. Here, we focus on the evolution
107 of macroscopic size in the five replicate anaerobic populations. Yeast in this treatment increased
108 their mean cluster radius from 16 μm to 434 μm, a ~$2 \cdot 10^4$-fold increase in volume (Fig. 1E, $p <$
109 0.0001; $F_{5,\ 13321} = 2100$, Dunnett's test in one-way ANOVA). This corresponds to an estimated
110 increase from ~100 cells per cluster to ~450,000 (comparing average cluster volumes, accounting
111 for changes in mean cell volume and cellular packing density within clusters).

112 The largest clusters of 600-day evolved macroscopic snowflake yeast are over a millimeter
113 in diameter (Fig. 1C), which is comparable to the size of an adult *Drosophila*[29]. Much like their
114 microscopic snowflake yeast ancestor[18,28], macroscopic snowflake yeast possess a life cycle in
115 which groups of cells both grow in size and reproduce, generating multicellular propagules, over
116 the course of the ~24 h culture period (Extended Data Fig. 2). This analysis establishes that group
117 size is heritable, and our time series data (Fig. 1E) show every replicate population evolved to
118 form larger clusters at each 200-day sampling interval, strongly suggesting that larger size is an
119 adaptive trait evolving in response to settling selection. To test this hypothesis, we performed a
120 fitness assay competing the microscopic ancestor against each t600 PA1-5 population, under our
121 standard selective conditions of growth and settling selection. The 600-day evolved macroscopic
122 snowflake yeast were far more fit than their ancestor (mean daily selection rate constant = 2.5, Fig.
123 1F), increasing from a mean starting frequency of 52% to 99.9% over just three days.

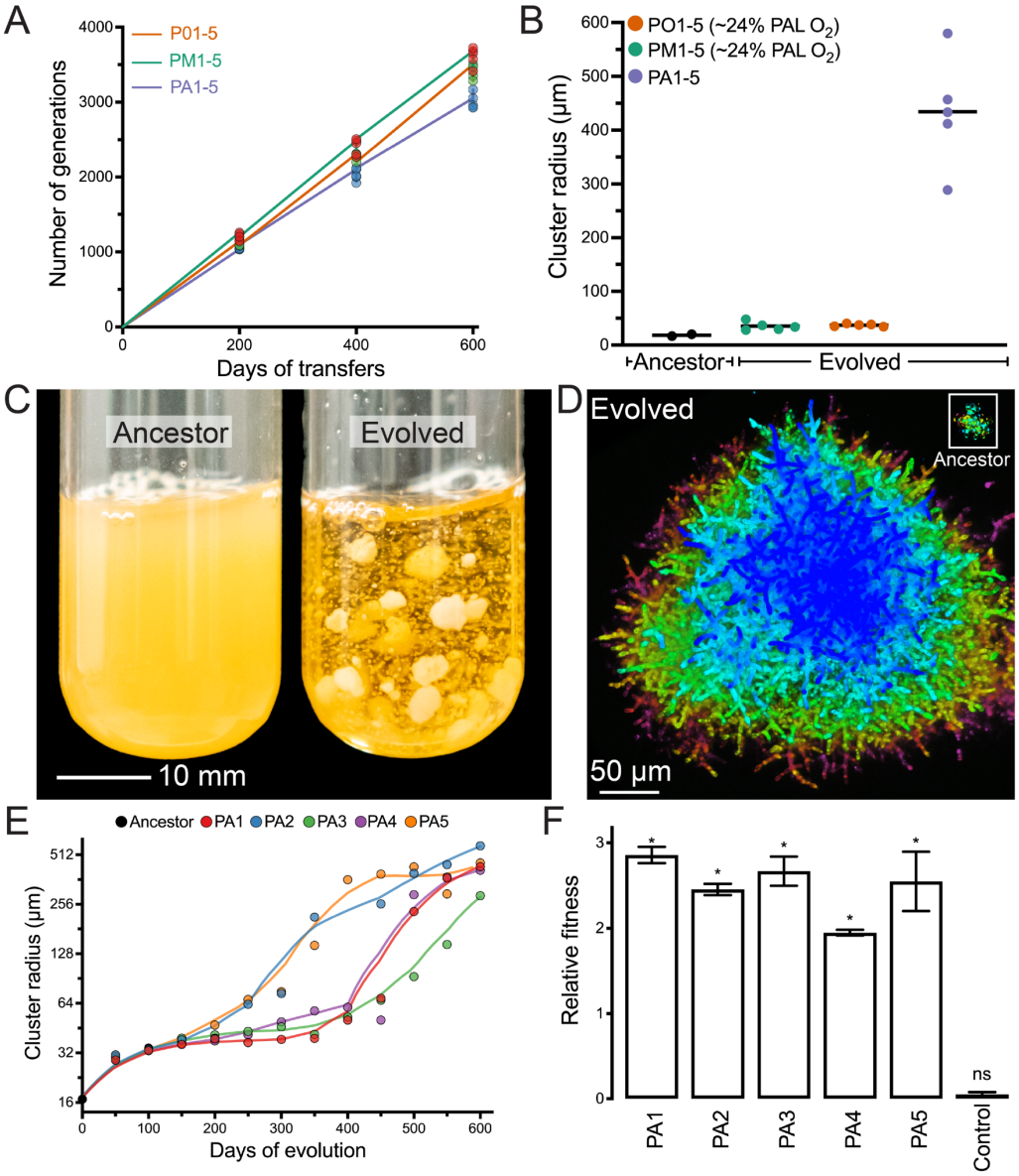

Figure 1. Evolution of macroscopic multicellularity in five replicate snowflake yeast populations. (A) We selected for larger size over 600 daily transfers, which represents ~3,000 generations. (B) Only the anaerobic populations (PA1-5) evolved macroscopic size over this time. (C) Individual snowflake yeast clusters from t600 are visible to the naked eye. (D) Representative clusters of the same two genotypes (ancestor in the upper right corner) shown under the same magnification (color represents depth in the *z* plane). (E) Temporal dynamics of size evolution in the anaerobic treatment (PA). (F) Macroscopic snowflake yeast were considerably more fit (calculated as a per-day selection rate constant (2.5)[30]) than their microscopic ancestor (n=3, error bars represent the SEM, asterisks denote significance at the 0.05 level). In A and E, the data points show the biomass-weighted mean radius (see Methods for details). See Extended Data Fig. 1 for additional data on the evolution of cluster size in oxygen-using populations (PM and PO) and Extended Data Fig. 3 for cluster size distributions for the 600-day anaerobic populations (PA1-5). Lines in (E) are Lowess smoothing curves intended to aid the eye.

138 As with their ancestor, macroscopic snowflake yeast grow via incomplete mother daughter
139 cellular separation, forming a branched, tree-like structure (Fig. 2A&B). When compressed,
140 macroscopic clusters fracture into small modules that resemble microscopic snowflake yeast in
141 terms of branching morphology (Fig. 2 A&B). Their cellular morphology, however, changed
142 markedly. Throughout the experiment, snowflake yeast cells evolve to be more elongate across all
143 five replicate populations, increasing in average aspect ratio (ratio of length to width) from ~1.2
144 to ~2.7 (Fig. 2C&D; $F_{5, 1993} = 206.2$, $p < 0.0001$, Dunnett's test after one-way ANOVA; Extended
145 Data Fig. 4). Even in macroscopic snowflake clusters, cell size and shape did not depend on
146 location in the cluster (*i.e.*, interior or exterior; Extended Data Fig. 5). Initially, cluster size was a
147 roughly linear function of cellular aspect ratio (Fig. 2E inset), but this relationship changes once
148 they evolve macroscopic size (Fig. 2E).

149 Prior work has shown that the evolution of more elongate cells increases the size to which
150 microscopic snowflake yeast grow by decreasing the density of cellular packing (*i.e.*, their packing
151 fraction) in the cluster interior, which reduces cell-cell collisions that drive multicellular
152 fracture[18,31]. To establish a null expectation for the effect of cell aspect ratio on cluster packing
153 fraction, we simulated the growth of individual clusters from a single cell using an experimentally-
154 validated model (see methods for details)[18]. In these simple 3D simulations, cellular packing
155 fraction decreased monotonically with increasing cellular aspect ratio (Fig. 2F). We then examined
156 this relationship over the course of our long-term experiment in replicate population two (PA2),
157 which was one of the first lineages to evolve macroscopic size. As predicted by our simulation,
158 cellular elongation decreased the packing fraction of microscopic multicellular groups− but only
159 initially, from aspect ratio ~1.2-2.0. Beyond this, clusters with more elongate cells actually became
160 more densely packed, and experimentally-measured packing fraction became increasingly

divergent from model predictions (Fig. 2F). This divergence suggests that this lineage evolved a novel biophysical mechanism for increased multicellular toughness, capable of withstanding growth to macroscopic size and a high cellular packing fraction.

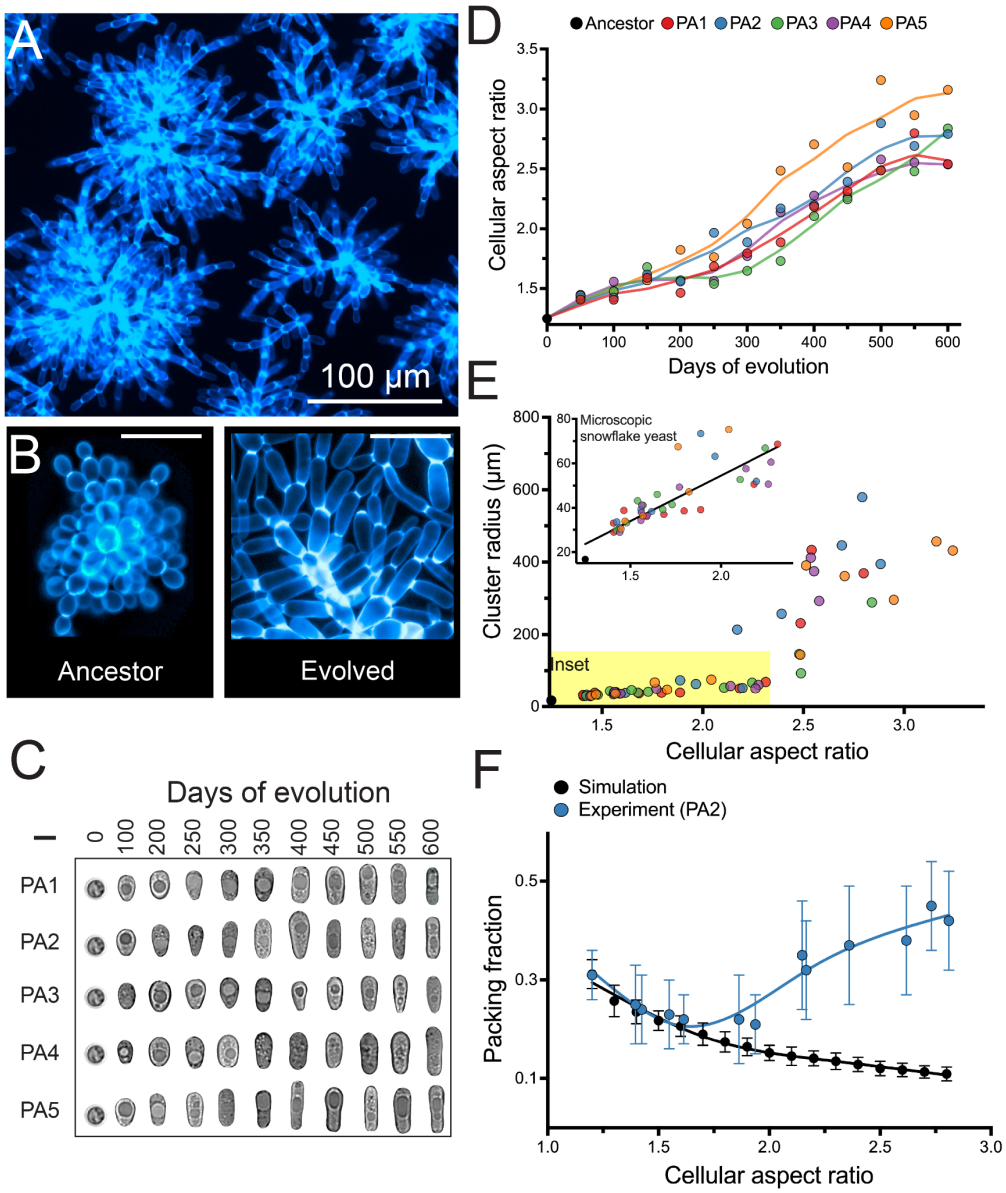

Figure 2. Evolution of novel cell morphology. (A) When compressed, macroscopic snowflake yeast fracture into modules, retaining the same underlying branched growth form of their microscopic ancestor as seen in (B) (scale bars are 20 µm). Cell walls are stained with calcofluor-white in (A) and (B). (C) and (D) show the parallel evolution of elongated cell shape, resulting in an increase in average aspect ratio from ~1.2 to ~2.7 (for each point in D, 453 cells were measured on average. The t0 ancestor is the same for PA1-5. Scale bar in C is 5 µm). An expanded version of (C) is shown in Extended Data Fig. 6. (E) Early in their

evolution (aspect ratio 1-2.3), cluster size (weighted mean radius) is an approximately linear function of cellular aspect ratio (inset; $p < 0.0001$, $y = 41.1x - 27.8$, $r^2 = 0.72$). This relationship does not hold beyond aspect ratio ~2.5. (F) A biophysical model of snowflake yeast predicts that increasing cellular aspect ratio should decrease cellular packing fraction (black points). We see a close correspondence with these predictions for low aspect ratios, but our experimental data diverges from model predictions for aspect ratios beyond 2. Each datapoint in (F) reports the mean of 15 snowflake yeast clusters or 25 replicate simulations, ± one standard deviation.

The simplest way that snowflake yeast could evolve to become macroscopic is to become adhesive, forming large aggregates of many separate snowflake yeast clusters. Indeed, aggregation is a common mechanism of group formation in yeast (i.*e.*, via flocculation[32]), and this would explain the modular structure of macroscopic snowflake yeast (Fig. 2A). To determine if clusters of macroscopic yeast form via aggregation, or if they develop as a single clonal lineage, we labeled a single-strain isolate (taken from PA2 after 600 days of selection), with either GFP or RFP. If adhesive aggregation were responsible for their large size, we would expect to see chimeric groups composed of both red and green-fluorescent sub-clusters[32]. After five rounds of co-culture, however, all multicellular clusters (n=70; Extended Data Fig. 7) remained monoclonal. This is unlikely to occur with aggregation. If we conservatively assume each macroscopic snowflake yeast cluster we measured was the result of just a single fusion event, occurring with equal probability between two groups of red and green cells, then the binomial probability of finding no chimeric groups in our sample would be 10^{-6}. Floc-like aggregation thus does not explain the evolution of macroscopic size in snowflake yeast.

To examine how changes in the topology of macroscopic snowflake yeast may underlie their increased size, we imaged clusters via Serial Block Face Scanning Electron Microscopy (SBF-SEM). This technique enables us to image the interior of macroscopic clusters that are difficult to resolve with light-based microscopy, allowing us to map their internal architecture with nanometer precision[33]. Within macroscopic clusters, separate branches contact, intercalate, and

197 even wrap around each other (Fig. 3A). As these clusters are densely packed, moving one
198 component would require moving many other components as well. Further, we found that
199 individual macroscopic snowflake yeast were not composed of a single topologically-connected
200 component, like their ancestors. Instead, they contained disconnected branches of cells, suggesting
201 that the cluster remained intact even when cell-cell connections were broken (Fig. 3A). Based on
202 these observations, we hypothesized that branches of macroscopic clusters are entangled, in a
203 manner reminiscent of physical gels[34] and entangled granular materials[35]. Entanglement would
204 provide a mechanism for branches of cells to remain in the same, densely packed group even after
205 cell-cell bonds break.

206 Following prior work in entangled chains and knotted strings[35,36], we used our SBF-SEM
207 dataset to quantify branch entanglement in macroscopic snowflake yeast by analyzing chain
208 topology and geometry. Specifically, we constructed the convex hull of each connected component
209 within a sub-volume, which denotes the smallest convex polyhedron containing this component
210 (see Extended Data Fig. 8A). If a cell from one connected component overlaps with the convex
211 hull of a second, then the two can be considered entangled. By percolating entanglement among
212 adjacent connected components throughout the sub-volume, we can measure the extent to which
213 the cluster's biomass is mutually entangled (Fig. 3B, Extended Data Fig. 8B). For entanglement
214 to underlie macroscopic size, the largest entangled component (consisting of many entangled
215 pieces) must be able to resist mechanical stress, meaning that there must be an entangled
216 component that spans the vast majority of the cluster[37]. In analyses of 10 randomly selected sub-
217 volumes from different macroscopic snowflake yeast clusters from population PA2 t600
218 macroscopic yeast, we found that the largest entangled component contains 93% +/- 2% of all

219 connected components. This observation supports the hypothesis that entanglement between cell
220 branches can prevent cluster fracture in the event that a cell-cell bond fractures.

221 As a further test, we investigated the mechanics of macroscopic snowflake yeast. Entangled
222 materials are known to exhibit two key mechanical signatures: strain stiffening and high material
223 toughness[35,38]. Strain stiffening describes the fact that, when compressed, the effective stiffness of
224 entangled chains increases with increased strain. By efficiently distributing stress across
225 constituent bonds, entangled materials can withstand stress orders-of-magnitude greater than their
226 non-entangled counterparts[38,39]. As the microscopic ancestor is presumably not entangled, it should
227 not exhibit strain-stiffening behavior or possess high toughness. We measured the mechanical
228 stress response of 10 macroscopic snowflake yeast clusters under uniaxial compression using a
229 macroscopic mechanical tester (Zwick Roell Universal Testing Machine). We repeated the same
230 experiment for 10 ancestral microscopic snowflake yeast clusters using an atomic force
231 microscope (AFM Workshop LS-AFM). The stress-strain plot for the microscopic ancestor is
232 linear ($r^2 = 0.97$ +/- 0.02, average and standard deviation of the regression for 10 samples, Fig. 3C
233 inset), clusters fracture at stress as low as 240 Pa and have toughness as low as 8.9 J/m^3 [18]. By
234 contrast, macroscopic snowflake yeast clusters have a convex stress-strain curve (Fig. 3C), can
235 support stresses at least as large as ~7 MPa without failing, and have toughness greater than 0.6
236 MJ/m^3. Thus, entanglement both enables separate branches within macroscopic snowflake yeast
237 to stay together and allows them to endure the large stresses necessary for growth to macroscopic
238 size.

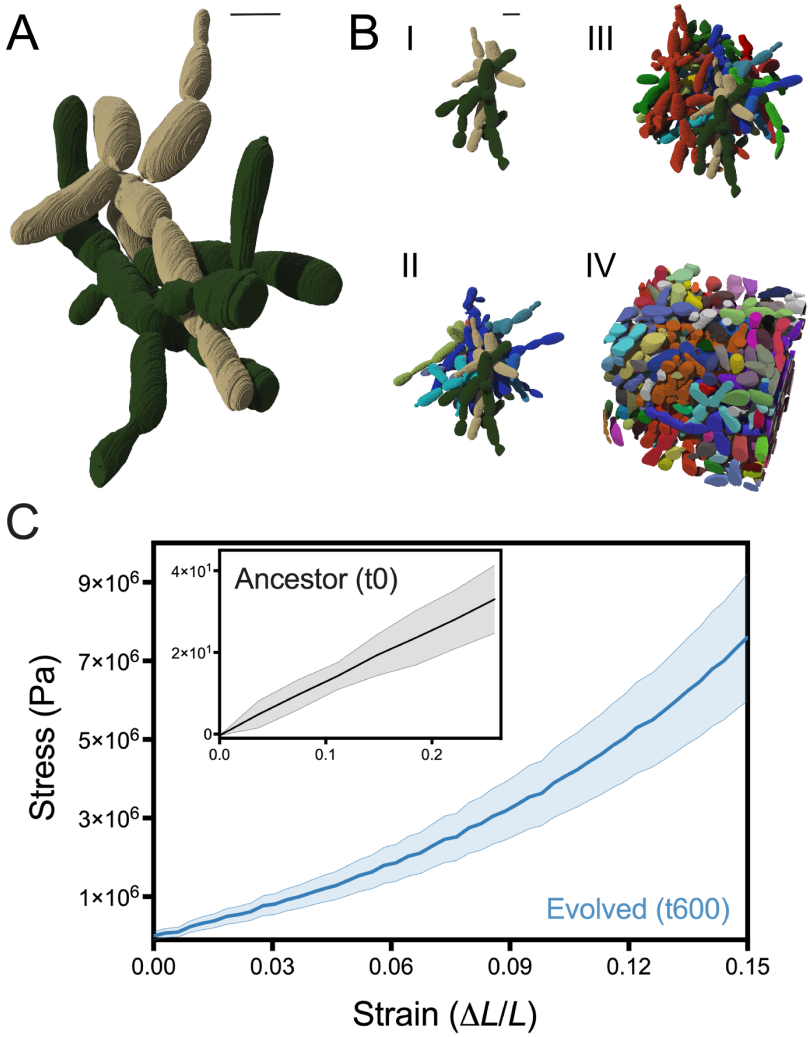

Figure 3. Branch entanglement underlies the evolution of macroscopic size. (A) Shown are two entangled components (green and tan), obtained via SBF-SEM imaging. (B) Branch entanglement is pervasive in macroscopic snowflake yeast. Starting with the two-component sub-volume in (A), we percolated entanglement by adding on adjacent entangled components in four steps (I-IV). Scale bars on A and B are 5 µm. (C) Stress vs. strain plot for macroscopic snowflake yeast (PA2, t600) clusters in blue and the ancestor in grey (ancestor shown again in inset with a rescaled *y* axis). Macroscopic snowflake yeast experience strain stiffening, a hallmark of entangled systems, while the ancestor's stress-strain plot is linear, which is expected for non-entangled systems. The shaded area shows one standard deviation based on 10 repeated measurements for each.

To rule out alternative hypotheses, we made additional measurements on macroscopic snowflake yeast (PA2 t600) and their microscopic ancestor. First, we measured the stiffness of individual cells to determine if they were becoming tougher. We did not detect a change between than ancestor and t600 macroscopic strain (0.018 and 0.019 N/m for the ancestor and evolved, respectively, Extended Data Fig. 9a). To determine if, in the absence of macroscopic entangled structures, individual PA2 t600 cells still show strain stiffening behavior, we crushed macroscopic clusters into smaller, microscopic branches before compressing them. These small groups displayed a linear stress-strain curve like their unevolved microscopic ancestor. In the absence of their macroscopic phenotype, the cells of the PA2 t600 yeast do not behave like an entangled material (Extended Data Fig. 9B).

Finally, we performed a positive control: we created persistently entangled groups experimentally. As described in Extended Data 7, growth in well-mixed liquid media prevents the formation of chimeric groups through entanglement. Yet if entanglement is critical for multicellular toughness, allowing fractured branches to remain in the same group, then chimeric clusters held together only by entanglement should be possible to grow under the right environmental conditions. We allowed GFP and RFP-tagged versions of PA2 t600 to grow at high density on solid media for 48 h, then cultured these yeast in liquid media for two rounds of growth and settling selection. These yeast readily formed and maintained chimeric groups. Specifically, 30% (31/101) of the clusters of the macroscopic genotype were still chimeric, with visibly entangled branches of green and red yeast (Extended Data Fig. 10). In contrast, only 1/110 clusters of the ancestral genotype were chimeric when cultured under the same conditions (0.9%, $p < 0.001$, $t = 6.59$, df = 209, two-tailed t-test). Taken together, this experiment shows that entanglement allows evolved snowflake yeast to remain intact, even when constituent branches lack continuous

272 mother-daughter cellular bonds (*i.e.*, red and green branches are not attached to each other by
273 permanent bonds).

274 To uncover the genomic basis of cell-level changes underlying multicellular adaptation,
275 we sequenced the genomes of a single strain from each of the five populations (PA1-PA5) that
276 independently evolved macroscopic multicellularity after 600 transfers (Fig. 4A&B). Over ~3,000
277 generations, snowflake yeast in our anaerobic treatment evolved dramatically more elongate cells
278 (Fig. 2C&D), which plays a central role in the evolution of increased cluster size (Fig. 2E) and
279 biophysical toughness (Figs. 2F & 3). Gene Ontology (GO) terms associated with cell length were
280 significantly enriched, namely genes of the cell cycle[40] (29 / 123 mutations, p = 0.02) and
281 filamentous growth (7 / 123 mutations). In addition, we found 11 nonsynonymous mutations in
282 genes with known roles in cellular budding (Fig. 4D), which includes eight genes that have
283 previously been shown to increase the size of the bud neck (*AKR1*, *ARP5*, *CLB2*, *GIN4*, *PRO2*,
284 *RPA49*, *RSC2*, *PHO81*)[41,42]. Mutations arose in two of these genes in different populations (*i.e.*,
285 *PHO81* in populations PA1 and PA5, and *GIN4* in populations PA2 and PA3, Fig. 4C), indicating
286 parallel evolution. Larger bud scars should increase the amount of cell wall connecting cells,
287 increasing the strength of the bond and toughness of the group. In our ancestral strain Y55, *gin4Δ*
288 cells formed bud necks that had a 1.7-fold larger cross-sectional area (t=2.8, df = 8, p < 0.01).
289 Consistent with this, we found that PA2-t600 macroscopic snowflake yeast evolved to form bud
290 necks that had a 2.4-fold larger cross-sectional area (t = 5.3, df = 24, p < 0.001), and bud scars that
291 were 5.8x larger 3D volume (t = 7.3, df = 24, p < 0.001) than their microscopic ancestor (Extended
292 Data Fig. 11).

293 As a final proof of principle, we set out to show that cellular elongation, aided by increased
294 cell-cell bond strength, is sufficient to underpin the origin of macroscopic size in snowflake yeast.

295 Starting with the microscopic *ace2Δ* ancestor, we deleted the cyclins *CLN3* and *CLB2* in order to
296 artificially increase cellular aspect ratio, and deleted *GIN4* to increase bud scar size, and thus
297 strength. *CLN3*, while not present in evolved isolates, has a large, well-understood phenotypic
298 effect on cell shape. Deleting *CLN3* and *CLB2* increased cellular aspect ratio (AR) by 21% and
299 45% respectively in single mutants, and 95% in the double mutant, with *GIN4* deletion further
300 increasing the aspect ratio of each genotype in addition to its effects on bud scars (Fig. 4E and F).
301 Our results mirror those from our evolution experiment: strains with AR < 2.5 were clearly
302 microscopic, with increasing AR resulting in a gradual increase in group size. At AR ~2.5, *ace2Δ*
303 *clb2Δ cln3Δ* yeast were at the threshold of macroscopic size, but still quite a bit smaller than our
304 t600 isolates. The *ace2Δ clb2Δ cln3Δ gin4Δ* mutant, with an AR of 3.7, formed well-developed
305 macroscopic clusters (Fig. 4F; experimentally-evolved strains described in Fig. 1E are shown in
306 gray to facilitate direct comparison).

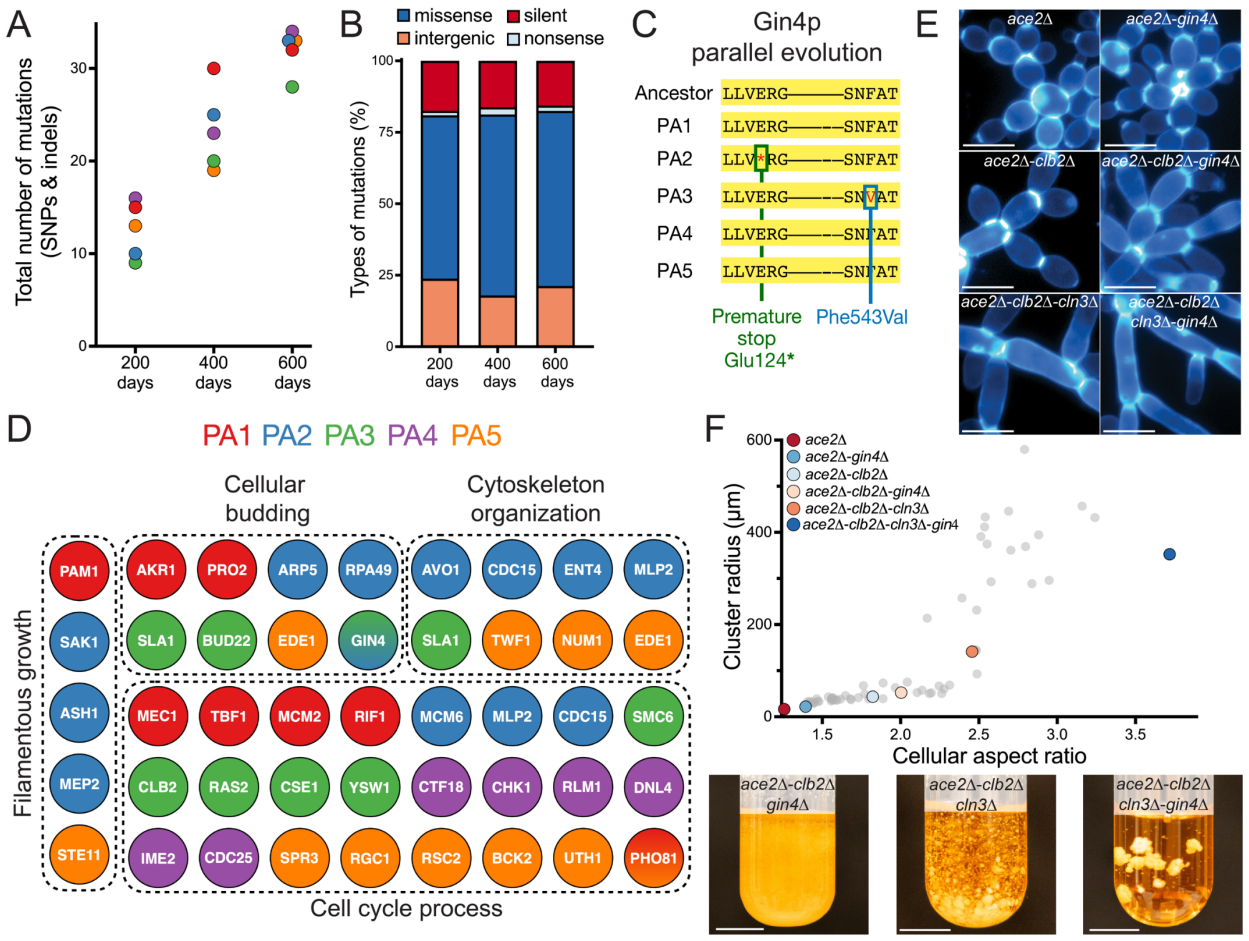

Figure 4. Whole-genome sequencing reveals the dynamics of molecular evolution and the genetic basis of cell-level and cluster-level changes. (A) and (B) show the number and types of mutations in evolved single strains from each population. (C) *GIN4*, a kinase whose loss of function increases bud neck size, is mutated in two independent populations. (D) Macroscopic snowflake yeast were enriched in mutations affecting cell cycle progression, cytoskeleton, and filamentous growth. In addition, we saw mutations affecting budding (*i.e.*, the location of buds on the cell surface, and bud neck size). These constituted 11 non-synonymous mutations out of the 123 total mutations in genotypes isolated from PA1-PA5 after 600 days of evolution. (E) Representative images of cells from strains used to re-engineer macroscopic size. Scale bars are 10 μm. (F) Engineered strains recapitulated the evolutionary trajectory established over 600 rounds of selection. With cellular aspect ratio below ~2.5, snowflake yeast remained microscopic, greatly increasing in size beyond this threshold. Scale bars are 10 mm.

Discussion

In this paper, we show that snowflake yeast, a model system of undifferentiated multicellularity, were capable of sustained multicellular adaptation, evolving macroscopic size over 600 days of experimental evolution. Macroscopic snowflake yeast are readily visible to the naked eye, containing hundreds of thousands of clonal cells. They achieved this remarkable increase in size by evolving highly elongate cells that become entangled within the cluster interior. This critical innovation allows multicellular groups to remain physically attached even when individual cellular connections are severed, increasing cluster toughness by more than 10,000-fold. As a material, snowflake yeast evolve from being ~100-fold weaker than gelatin[43], to having the strength and toughness of wood[44]. Sequencing revealed an enrichment in mutations affecting the cell cycle and budding - traits that increase cell length and the amount of cell wall material at the point of attachment. Engineered strains with mutations increasing cell length and bud scar size recapitulated our evolutionary progression from microscopic to macroscopic size.

In our system, novel multicellular traits arise as an emergent property of changes in cell-level traits. Two cell-level innovations appear to have played a key role in the evolution of macroscopic size: more elongate cells and larger bud scars. Increased cell length initially reduces the strain generated from cellular packing, which is the primary manner in which size increased early in the experiment, and may underlie entanglement by facilitating cellular intercalation. Larger bud scars increase the amount of shared cell wall connecting cells, which all else equal should increase multicellular toughness by strengthening cell-cell bonds[31]. While the evolution of larger, tougher multicellular groups necessarily has underlying cell-level causation, these group and cell-level traits are distinct and non-commensurable (*i.e.*, group size and toughness cannot be measured at the single-cell level). This demonstrates that snowflake yeast are evolving under

342 MLS2, a shift in evolutionary dynamics that is critical for the transition multicellular individuality,
343 as it allows groups as a whole, not just their constituent members, to gain adaptations[45,46].

344 Entanglement is a common mechanism through which filamentous materials can solidify.
345 It can operate on nearly any length scale, ranging from nanoscale polymers[47] and nanofibers[48], to
346 macroscopic staples[49], and beaded chains[50]. Relatively little is known about the role of
347 entanglement in the materials properties of macroscopic biological structures, though recent work
348 has shown that California Blackworm collectives are entangled, and can vary their degree of
349 entanglement to solidify and melt their groups in response to environmental change[51-53].
350 Macroscopic multicellularity has evolved repeatedly in fungi[54], and while to our knowledge no
351 prior work has formally examined whether the cells of fungal fruiting bodies and lichen thalli are
352 physically entangled, they are generally composed of densely-packed, overlapping hyphae,
353 strongly suggesting entanglement[55-57]. The prevalence of entanglement in superficially different
354 systems is likely due to its simplicity and efficacy; if pairs of constituents are easily entangled,
355 large mutually-entangled clusters readily form, greatly increasing the strength and toughness of
356 the material. While further work will be required to test this hypothesis, the relative ease with
357 which multicellular fungi form entangled structures may have facilitated the highly convergent
358 evolution of macroscopic multicellularity within this clade[54], allowing different fungal lineages to
359 independently evolve robust multicellular structures.

360 Our results depend on the fact that snowflake yeast grow as topologically-structured groups
361 with permanent cellular bonds, and we would not necessarily expect similar biophysical exaptation
362 in organisms with alternative means of group formation. These features, however, make it well
363 suited as a model system for the lineages that have ultimately evolved complex multicellularity.
364 Of the five lineages that independently evolved complex multicellularity (fungi, animals, plants,

365 red algae, and brown algae), all but animals possess permanent cell-cell bonds, and early
366 multicellular lineages in each are thought to have started out as simple, topologically-structured
367 networks[58]. While animals do not currently have permanent cell-cell bonds, little is known about
368 their ancestral mode of cellular adhesion. Indeed, their closest living relatives, the
369 choanoflagellates, can form topologically structured multicellular groups with permanent cell-cell
370 bonds[59-61], suggesting that early animals may have possessed a similar mode of growth.

371 Despite 600 rounds of selection for increased size, our mixotrophic and obligately aerobic
372 lineages remained microscopic (Fig. 1C & Extended Data Fig. 1), increasing their radius by less
373 than two-fold. Extending prior work examining the role of oxygen diffusion in the evolution
374 multicellular size[4], these results highlight the importance of environmentally-dependent tradeoffs
375 on the evolution of multicellularity. Oxygen can serve as a resource, allowing increased cellular
376 growth by increasing ATP yields from metabolism[62] and allows growth on non-fermentable carbon
377 sources[63]. For simple, diffusion-limited organisms like snowflake yeast, low concentrations of
378 oxygen create a cost to large size by reducing the proportion of cells in the group that have access
379 to it- a cost which our anaerobic populations did not face.

380 During the evolutionary transition to multicellularity, groups of cells must become
381 Darwinian entities capable of adaptation[64,65]. This requires that they reproduce, and have heritable
382 variation in traits that affect fitness[66]. For groups of cells to become more than simply the sum of
383 their parts, adaptation must take place in multicellular traits that are distinct from those of their
384 constituent cells (*i.e.*, they must evolve under MLS2)[45,46]. Until now, it has not been clear if simple
385 groups of cells are capable of making this transition, or whether they first require innovations that
386 allow for the heritable expression of novel multicellular traits[67,68]. Using long-term experimental
387 evolution, we show even simple groups of cells, initially differing from their unicellular ancestor

388 by a single mutation, have an innate capacity for open-ended multicellular adaptation. In response
389 to selection on group size, a broadly important trait for simple multicellular organisms[69], snowflake
390 yeast evolved to form radically larger and tougher multicellular groups by leveraging the emergent
391 biophysical properties of altered cellular morphology. These results demonstrate how selection on
392 group size can drive sustained multicellular adaptation and biophysical innovation, and highlight
393 the surprising ease with which evolutionary transitions in Darwinian individuality can occur.

394 **Methods**

395 **Long-term evolution experiment.** To generate our ancestral snowflake yeast for the MuLTEE,
396 we started with a unicellular diploid yeast strain (Y55). In this yeast, we replaced both copies of
397 the *ACE2* transcription factor using a *KANMX* resistance marker (ace2::*KANMX*/ace2::*KANMX*)
398 and obtained a snowflake yeast clone (see[28] for a detailed description of strains and growth
399 conditions, including measurements of oxygen concentrations in growth media). When grown in
400 YEPD media (1% yeast extract, 2% peptone, 2% dextrose), these yeast are mixotrophic, both
401 fermenting and respiring. When grown in YEPG media, which is the same as YEPD but with the
402 dextrose replaced by 2.5% glycerol, these yeast are incapable of fermentation and are obligately
403 aerobic. From this initial clone of *ace2Δ* snowflake yeast, we selected a randomly produced 'petite'
404 (p^-) mutant. Due to a large deletion in its mitochondrial DNA (identified via sequencing), this
405 snowflake yeast is unable to respire and is therefore metabolically 'anaerobic,' and was cultured
406 in YEPD.

407 We evolved five replicate populations of mixotrophic snowflake yeast (referred to as
408 populations PM1-PM5), obligately aerobic (PO1-PO5) and anaerobic (PA1-PA5) snowflake yeast
409 in 10 mL of culture media, growing them in 25 x 150 mm culture tubes for 24 hours at 30°C with
410 225 rpm shaking. We used settling selection to select for larger cluster size. Once per day, after
411 ~24 h of growth, we transferred 1.5 ml of culture into 1.5 mL Eppendorf tubes, let them settle on
412 the bench for 3 minutes, discarded the top 1.45 mL of the culture, and only transferred the bottom
413 50 µl of the pellet into a new 10 mL of culture media for the next round of growth and settling
414 selection. Once the anaerobic populations (PA1-PA5) had started to evolve visibly larger clusters
415 with all biomass settling to the bottom of the tube in under a minute, we decreased the length of
416 gravitational selection to 30 seconds, thus keeping them under directional selection for increased

417 size. The timing of this change corresponded to ~350 days for PA2 and PA5 and ~500 days for
418 PA1, PA3, and PA4. We used wide-bore filtered pipette tips (Thermo Scientific) for our daily
419 transfers. In total, we applied 600 rounds (days) of growth and settling selection. We archived a
420 frozen glycerol stock of each population at -80°C every 10-15 transfers.

421 **Measuring cluster size.** We developed a standard visualization protocol to be able to measure the
422 size of both microscopic and macroscopic snowflake yeast from each population over the 600-day
423 evolution experiment. To prepare yeast for imaging, we revived evolved frozen cultures for each
424 population in 50-day intervals (12 for each of the 15 replicate populations). We then inoculated
425 each sample into 10 mL fresh media and brought them to equilibrium over a five-day culture
426 process, performing daily settling selection prior to transfer to fresh media. After 5 transfers, we
427 pipetted a random 1mL subsample of each 24-hour culture, placing them in 1.5 ml Eppendorf
428 tubes. We added 0.5 ml of sterile water to each well of 12-well culture plates, then gently vortexed
429 each snowflake yeast sample and diluted them into the water (1,000-fold dilution for microscopic
430 populations, and 100-fold dilution for macroscopic populations). We shook each well plate gently
431 to disperse the yeast clusters evenly over the bottom of each well. We then imaged each well using
432 a 4X Nikon objective, capturing the cross-sectional area of clusters without disrupting their 3D
433 structure. Next, we used ImageJ-Fiji to calculate the cross-sectional area of each cluster,
434 converting pixels to microns by including a physical 100 μm scale bar in each image.

435 **Calculating weighted average cluster size.** The distribution of cluster size across various isolates
436 are not consistent- while microscopic populations are unimodal, while macroscopic populations
437 contain a substantial number of small groups that may only contain a few cells. Even when these
438 small groups constitute a trivial amount of the population's biomass, variation in their abundance
439 can have a large impact on sample statistics, like average cluster size. Because of their skewed size

440 distribution, mean size is an unreliable and often uninformative measure of the central tendency
441 of the cluster size distribution, and does not accurately describe how cells are distributed across
442 different cluster size classes. To account for this, we calculated the distribution of cellular biomass
443 over the range of cluster sizes, and found the mean of this biomass distribution (which is the same
444 as weighting mean cluster size by its biomass). This weighted mean cluster size represents the
445 expected size group any given cell will be in (see Extended Data Fig. 2 for a visual representation),
446 and is an accurate measure of changes in the distribution of cellular biomass across different cluster
447 sizes over evolutionary time. Rather than presenting the weighted mean group size as a volume,
448 we transformed these into an average (micron) radius to be consistent with the units that have
449 historically been used in the paleontological literature documenting the evolution of macroscopic
450 multicellular organisms.

451 **Assessing fitness.** We measured the relative fitness of the evolved macroscopic populations (PA1-
452 5) in competition against the ancestor in liquid culture under the same conditions as our evolution
453 experiment. To differentiate competing strains, we used an ancestral snowflake yeast strain
454 carrying a hemizygous red fluorescent protein (*ura3::dTOMATO/URA3*). Before coculturing these
455 strains, we first grew evolved populations and the ancestral strain in separate cultures overnight.
456 Then we mixed the two types in a 1.5 mL microcentrifuge tube to start the competition assay in
457 fresh 10 mL YEPD cultures. We examined the fitness of PA1-5 t600, as well as an
458 ancestor:ancestor control, with three replicate competitions per treatment. We grew these
459 competitions for 24 hours in 10 mL YEPD (conditions as described in the evolution experiment),
460 followed by 3 minutes of settling selection in 1.5 mL Eppendorf tubes. We then transferred the
461 bottom 50 µl into a fresh culture tube for the next round of growth and settling, repeating the same
462 procedure for three rounds across the fitness assay. The evolved populations' initial frequency

463 ranged between 35-70%, and after three rounds of growth and settling selection, they reached a
464 range between 99.8-99.9%.

465 To calculate the relative fitness of the evolved populations against the common ancestor,
466 we calculated their selection rate constant, as described in [30]. To do so, we estimated the initial and
467 final cellular density of yeast by measuring the cross-sectional area of the evolved and ancestral
468 snowflake yeast clusters at the beginning and end of the fitness assay using a Nikon Eclipse Ti
469 inverted microscope at 100x magnification. Then we calculated the selection rate by dividing the
470 estimated density of the evolved populations at the end and beginning of the competition assay,
471 followed by subtracting the natural log of this value from that of the ancestral strain[30]. Finally, by
472 coculturing the ancestral snowflake yeast strains with and without the hemizygous *dTOMATO*
473 constructs, we confirmed that the expression of this protein had no significant fitness cost, as
474 reported in Fig1F, right column ($p=0.22$, $t=1.7$, $df=2$, one sample t-test). Image analysis was
475 performed in ImageJ (v2.3.0).

476 **Aspect ratio data collection and analysis.** To measure the evolution of cellular aspect ratio in
477 populations PA1-PA5 over the 600-day evolution experiment, we first inoculated 61 samples (1
478 ancestor + 5 replicates x 12 time points, each separated by 50 days) and grew them overnight in
479 shaking incubation as described above. Following the same growth protocols as in our cluster size
480 measurements, we grew these samples for five consecutive days with settling selection. On the
481 final day, we transferred 100 µl of each culture into tubes with fresh YEPD and incubated them
482 for 12 hours. Next, we stained samples in calcofluor-white by incubating them in the dark for 30
483 minutes (at a final concentration of 5 µM) prior to imaging (40x objective, UV excitation of blue
484 fluorescent cell wall stain, imaged on a Nikon Ti-E). We measured the aspect ratio of individual

485 cells within snowflake yeast clusters on ImageJ-Fiji, analyzing an average of 453 cells per
486 population.

487 **Simple biophysical model examining packing fraction as a function of aspect ratio.** We
488 simulated the growth of snowflake yeast from a single cell. Cells were modeled as prolate
489 ellipsoids with one long (major) axis and two equal shorter (minor) axes. Clusters started as a
490 single cell and were grown for nine cellular generations. New cells first emerged from their
491 mother's distal pole; subsequent cells emerged with a polar angle of 45° and a random azimuthal
492 angle. If adding a new cell would cause too much overlap with existing branches, the new cell was
493 deleted and the mother cell lost its chance to reproduce that generation. We simulated the growth
494 of 50 clusters of each genotype, which varied in their cellular aspect ratio, defined as the ratio of
495 the major axis to minor axis length, ranging from 1.2-2.8. We then calculated each simulated
496 cluster's packing fraction by fitting a convex hull to the cluster, and measuring the ratio of the total
497 volume to the volume specifically occupied by cells. The MATLAB code to grow snowflake yeast
498 using this protocol is attached as Supplementary File 1.

499 **Testing aggregative vs. clonal development.** To determine if macroscopic snowflake yeast
500 aggregate or develop clonally (Extended Data Fig. 7), we isolated a single genotype from PA2,
501 t600 (strain GOB1413-600), and engineered it to constitutively express either green or red
502 fluorescent proteins. To do that, we amplified the *prTEF_GFP_NATMX* construct from a pFA6a-
503 eGFP plasmid and the *prTEF_dTOMATO_NATMX* construct from a pFA6a-tdTomato plasmid.
504 We then separately replaced the *URA3* open reading frame with *GFP* or *dTOMATO* constructs in
505 an isogenic single strain isolate following the LiAc transformation protocol[70]. We selected
506 transformants on Nourseothricin Sulfate (Gold Biotechnology Inc., U.S.) YEPD plates and
507 confirmed green or red fluorescent protein activity of transformed macroscopic clusters by

508 visualizing them under a Nikon Eclipse Ti inverted microscope. To test whether they grow clonally
509 or aggregatively, we first inoculated *GFP* or *dTOMATO* expressing clones individually overnight.
510 We then mixed the two cultures in equal volume and diluted 100-fold into a 10 mL fresh culture.
511 We co-cultured this mixed population for five days, transferring 1% of the population to fresh
512 media every 24 h. Finally, we washed this culture in 1 mL sterile water and visualized 70 individual
513 clusters under both red and green fluorescent channels, allowing us to count the number of
514 snowflake yeast clusters that were green, red, or chimeric.

515 We examined the potential for entanglement alone to allow for persistent interactions among
516 disconnected components (Extended Data Fig. 10) by crushing GFP- and RFP-tagged macroscopic
517 snowflake yeast (PA2-t600) into smaller groups, and then growing a mixture of them on the surface
518 of agar plates for 48 hours, potentially allowing branches of adjacent genotypes to entangle through
519 growth. We then scraped these populations and grew them in 10 mL YEPD (yeast-extract, peptone,
520 dextrose) media with shaking at 250 rpm for two 24 h rounds of growth and settling selection. We
521 imaged the resulting clusters under widefield microscopy (Nikon Ti-E), taking pictures of
522 individual clusters under bright field, green, and red channels, collecting data for a random sample
523 of clusters (101 for the PA2-t600, and 110 for the ancestor control). We analyzed the images in
524 ImageJ-FIJI, and any clusters that contained both green and red cells were scored as chimeric. The
525 images shown in Extended Data Fig. 10 were taken on a Nikon AR1 confocal, allowing better
526 view of the 3D structure of chimeric intercalation.

527 **Specimen preparation for Serial Bulk Faced Scanning Electron Microscopy (SBF-SEM).** We
528 fixed snowflake yeast in 2% formaldehyde (fresh from paraformaldehyde (EMS)) containing 2
529 mM $CaCl_2$, incubating at 35°C for 5 minutes followed by 2-3 hours on ice. Next, we incubated
530 these yeast for an hour in a solution of 1.5% potassium ferrocyanide, 0.15M cacodylate buffer, 2

531 mM $CaCl_2$, and 2% aqueous osmium tetroxide. This last step was performed on ice and under
532 vacuum. Finally, we washed our yeast and incubated them in thiocarbohydrazide solution (10 g /
533 L double-distilled water) for 60 minutes at 60°C, followed by en bloc uranyl acetate and lead
534 aspartate staining[71,72].

535 **SBF-SEM.** We imaged fixed yeast on a Zeiss Sigma VP 3View. This system has Gatan 3View
536 SBF microtome installed inside a Gemini SEM column. For this work, yeast clusters that were
537 embedded in resin were typically imaged at 2.5 keV, using 50-100 nm cutting intervals, 50 nm
538 pixel size, beam dwell time of 0.5-1 μsec and a high vacuum chamber.

539 **SEM Image analysis.** Images were initially in.dm3 format, which we converted to .tiff using
540 GMS3 software. We then cleaned the images and passed them through a gaussian filter in Python.
541 Using the interactive learning and segmentation toolkit (ilastik), we segmented images into 3 parts:
542 live cells, dead cell debris, and background. We then imported segmented HDF5 files in Python.
543 First, we identified connected cells using the nearest neighbor algorithm to identify connected
544 cells. We call a set of connected cells inside a sub-volume a connected component. Then, using a
545 3D extension of the gift-wrapping algorithm, we extracted the convex hull of each connected
546 component.

547 **Visualization of SEM images.** After segmenting images as described above, we created a mesh
548 of individual cells by dilating binarized images. After creating the surface mesh of each individual
549 cell using the mesh tool in Mathematica 12, we imported whole sub-volumes in Rhino6. Then we
550 manually identified cell-to-cell connections and colored each connected component differently.

551 **Volume fraction data collection and analysis.** We measured the packing fraction (proportion of
552 the cluster volume that is cellular biomass) by measuring the number of cells within a cluster, their
553 size, and the volume of the cluster, following the protocol described in Zamani et al. (2021)[73].

554 **Mechanical testing.** To test the response of ancestral clusters to uniaxial compression we
555 submerged individual clusters under water, and then compressed them using a Puima Chiaro
556 nanoindenter (Optics11, 19.5 um spherical glass probe). For mechanical measurements of
557 macroscopic snowflake yeast, we used a Zwick Roell Universal Testing Machine (UTM) with 5
558 N probe. As above, individual clusters were extracted from the growth tube and placed on the
559 testing stage while submerged under water.

560 **Preparing glass slides with attached cells.** We coated glass slides with Concanavalin A to make
561 a sticky glass surface to which individual cells could adhere. We started by preparing a 10 mg/mL
562 solution of ConA dissolved in sterile DI water, which can be stored at -20C. This stock solution
563 was diluted 1:10, and then 200uL of diluted solution was pipetted onto a glass slide in a sterile
564 environment. The slide was allowed to incubate for 5 min at room temperature, then washed with
565 sterile DI water twice, then left to aspirate dry in the hood. Cell cultures were inoculated (100 uL)
566 onto the glass surface and left to settle for 5 minutes.

567 **AFM measurements.** Prior to measuring the properties of individual cells with the AFM, we
568 restored ACE2 functionality to increase the frequency of single cells available for mechanical
569 testing. To do this, we reinserted a single copy of the ancestral *ACE2* allele fused with the antibiotic
570 resistance gene *HYGNT1* into the genome of the PA ancestor and PA1 t600 isolate under the
571 control of its native promotor using the LiAc/SS-DNA/PEG method of yeast transformation[69].
572 Transformants were then plated on YEPD agar plates (1% yeast extract, 2% peptone, 2% dextrose,

573 1.5% agar) supplemented with 200 mg l^{-1} of the antibiotic hygromycin B (Enzo Life Sciences).
574 All atomic force measurements used an atomic force microscope from Asylum Research that was
575 integrated with an inverted optical microscope (Nikon). For single-cell measurements, we used a
576 silicon nitride cantilever with a nominal stiffness of 0.06 N/m with an attached borosilicate glass
577 bead with diameter 2um (Novascan Technologies). The cantilever was measured via thermal
578 analysis to have a stiffness of 0.0593 N/m. For cluster-level measurements, we used tipless,
579 aluminum coated cantilevers that have a rectangular shape (length 225 um, width 40 um) that have
580 a nominal stiffness of 30 N/m (AppNano). For measurements, either single cells or entire clusters
581 were visually aligned with the cantilever probe, which was then moved at a velocity of 1 um/s to
582 compress the cell or cluster with increasing force.

583 **Chitin staining protocol.** We stained cells with calcofluor white via the following protocol. First,
584 we mixed 500uL of cell culture from the ancestor and PA2 t600 strains into the same tube. Then,
585 we sampled 150 uL (containing both the ancestor and t600 yeast clusters) from the mixed culture.
586 We removed the supernatant via an iterated process of centrifugation and pipetting media removal.
587 Then, we diluted 15 uL of 1 mg/mL calcofluor solution into 500 uL 1x Phosphate-buffered saline
588 solution (PBS) and mixed with the yeast pellet. We incubated the sample in darkness at room
589 temperature for 25 minutes, then we removed the calcofluor media via centrifugation and pipetting.
590 Finally, we added 200 uL 1x PBS on top of the pellet. 20 uL of this cell suspension was pipetted
591 onto a clean glass slide and covered with a coverslip for microscopy.

592 **Single Cell and Bud Scar Confocal microscopy.** We used a Nikon A1R confocal microscope
593 equipped with a 60x oil immersion objective to obtain z-stack images of individual cells stained
594 with calcofluor white. To track the location and size of bud scars, we wrote a MatLab script to
595 extract the brightest calcofluor signals, since the chitinous bud site region makes bud scars brighter

596 than the other portions of the cell wall. Brightness isosurfaces isolated the bud scars themselves,
597 and the brightness of each voxel contained within the isosurface was recorded to track the density
598 of chitin. Next, the isosurface points were rotated to the x-y plane by finding the principal axes of
599 the shape via principal component analysis. The rotated surface points were then used to calculate
600 the height and cross-sectional area of the bud scars.

601 **DNA extraction and genome sequencing.** To extract DNA for whole-genome sequencing, we
602 isolated clones from each of the evolved replicate populations of anaerobic yeast (*i.e.*, PA1-PA5)
603 and their common ancestor after 200, 400, and 600 days of evolution. To pick clonal isolates, we
604 diluted populations of snowflake yeast clusters in 1.5 mL tubes and plated them at a density of
605 100-200 colonies per plate. Next, we restreaked those initial single colonies onto fresh plates, thus
606 ensuring that each colony on a plate results from a single snowflake yeast cluster. Because
607 snowflake yeast grow clonally, we expected that these isolates would only represent a single clone
608 of cells, with no more variation than would be expected from any single cell isolate that grew into
609 a population, generating *de novo* mutation along the way (subsequent analysis of the genomes
610 confirmed this: we never saw evidence of >1 genotype present in any isolate). We inoculated these
611 16 samples in YEPD for 12 hours and extracted their genomic DNA using a commercially
612 available kit (Amresco, Inc. VWR USA). We measured the concentration of DNA with a Qubit
613 fluorometer (Thermo Fisher Scientific, Inc.). We prepared genomic DNA libraries for the 16
614 samples using NEBNext Ultra DNA Library Prep Kit for Illumina (New England Biolabs, Inc).
615 We quantified the quality of the genomic DNA library using the Agilent 2100 Bioanalyzer system
616 located at the Genome Analysis Core Laboratories at Georgia Institute of Technology (Agilent
617 Technologies, Inc). Finally, whole genomes were sequenced using the HiSeq 2500 platform

618 (Illumina, Inc) by the Genome Analysis Core Center located in the Petit Institute, Georgia Tech.
619 As a result, we obtained paired 150 bp (R1 & R2) FASTQ reads from two lanes (L1 & L2).

620 **Bioinformatic analysis.** For our bioinformatic analysis, we used the bash command-line interface
621 on a Linux platform. To identify *de novo* mutations (single nucleotide changes, or 'SNPs,' and
622 small insertion/deletions, or 'indels') in the ancestral and evolved genomes, we first filtered out
623 low-quality reads using a sliding window approach on Trimmomatic (v0.39). We aligned reads to
624 the yeast reference genome (S288C, SGD) using an algorithm in the BWA software package (*i.e.*,
625 BWA-MEM)[74]. Next, we used the genome analysis toolkit (GATK) to obtain and manipulate .bam
626 files[75]. Duplicate reads were marked using the Picard - Tools (MarkSuplicates v2.18.3). We called
627 SNPs using two different tools, i.e., GATK4 HaplotypeCaller (v4.0.3.0) and FreeBayes
628 (v1.2.0)[75,76]. We validated SNP calls by comparing results obtained by two independent tools. For
629 indels, we used the output from HaplotypeCaller. To filter variants according to their quality/depth
630 scores and generate an overview of the variant calling step's statistical outcome, we used
631 VCFTOOLS (v0.1.16)[77]. Finally, after manually checking each variant call by visualizing SAM
632 files and VCF files on Integrative Genomics Viewer (IGV)[78], we extracted *de novo* variants by
633 making a pairwise comparison of each VCF file of the evolved genomes against the VCF file of
634 the ancestral genome by using bcftools-isec (v1.10)[79]. Lastly, we annotated evolved mutations
635 using SnpEff (v4.3T)[80].

636 To search for gene ontology (GO) term enrichment for *de novo* mutations, we generated a
637 combined list of synonymous and nonsynonymous mutations within gene coding regions. We then
638 searched for enriched gene ontology terms using GO Term Finder and GO Slim Mapper on the
639 yeast genome database[81].

640 **Genetically engineering macroscopic snowflake yeast.** To genetically engineer snowflake yeast
641 strains with cell lengthening (*CLB2* and *CLN3*) and bud-scar strengthening (*GIN4*) mutations that
642 are shown in Fig. 4, we used homozygous unicellular (GOB76) and multicellular strains (GOB8).
643 To engineer each gene deletion, we first amplified hygromycin, nourseothricin, and G418
644 resistance marker cassettes from plasmids and individually transformed them into yeast cells (see
645 Supplementary Table 1 for genotypes, plasmids, and primers). Next, we induced sporulation of
646 individual heterozygous mutant strains (2% KAc), dissected tetrads, and obtained homozygous
647 deletions through auto-diploidization. By subsequent rounds of sporulation and inter-tetrad mating
648 on appropriate multi-drug plates, we generated double, triple, and quadruple mutant strains (Fig.
649 4 E&F). Finally, we quantified the cellular aspect ratio and cluster size (cross-sectional area) of
650 these mutants by imaging clusters under a Nikon Eclipse Ti inverted microscope, using the same
651 methods as previously described.

652 **Life-cycle experiment (Extended Data Fig. 2).** To characterize the life cycle of the ancestral
653 (microscopic) and evolved (macroscopic, PA2-600) snowflake yeast, we inoculated both strains
654 starting from frozen glycerol stocks. Then, we grew them under the conditions of the evolution
655 experiment for five rounds of growth and settling selection. Applying a five-day growth and
656 settling selection brings cultures to an equilibrium, reflecting the physiology and size distribution
657 observed during the evolution experiment. On the final day, we sampled from the growing cultures
658 at 0, 3, 6, 12, and 24 hours and measured the number, size, and volume of cultures using the same
659 methods described under "Measuring cluster size."

References

1 Godfrey-Smith, P. *Darwinian populations and natural selection*. (Oxford University Press, 2009).

2 Bourke, A. F. Principles of social evolution. (2011).

3 Knoll, A. H. The multiple origins of complex multicellularity. *Annual Review of Earth and Planetary Sciences* **39**, 217-239 (2011).

4 Bozdag, G. O., Libby, E., Pineau, R., Reinhard, C. T. & Ratcliff, W. C. Oxygen suppression of macroscopic multicellularity. *Nature Communications* **12**, 1-10 (2021).

5 Smukalla, S. *et al.* FLO1 is a variable green beard gene that drives biofilm-like cooperation in budding yeast. *Cell* **135**, 726-737 (2008).

6 Bonner, J. T. *The evolution of complexity by means of natural selection*. (Princeton University Press, 1988).

7 Bell, G. & Mooers, A. O. Size and complexity among multicellular organisms. *Biological Journal of the Linnean Society* **60**, 345-363 (1997).

8 Bonner, J. T. Perspective: the size-complexity rule. *Evolution* **58**, 1883-1890 (2004).

9 Willensdorfer, M. Organism size promotes the evolution of specialized cells in multicellular digital organisms. *Journal of evolutionary biology* **21**, 104-110 (2008).

10 Solari, C. A., Kessler, J. O. & Goldstein, R. E. A general allometric and life-history model for cellular differentiation in the transition to multicellularity. *The American Naturalist* **181**, 369-380 (2013).

11 Fisher, R., Shik, J. & Boomsma, J. The evolution of multicellular complexity: the role of relatedness and environmental constraints. *Proceedings of the Royal Society B* **287**, 20192963 (2020).

12 Knoll, A. H. & Hewitt, D. Phylogenetic, functional and geological perspectives on complex multicellularity. *The major transitions in evolution revisited*, 251-270 (2011).

13 Bonner, J. T. *Why size matters: from bacteria to blue whales*. (Princeton University Press, 2011).

14 Boudaoud, A. An introduction to the mechanics of morphogenesis for plant biologists. *Trends in plant science* **15**, 353-360 (2010).

15 Höhn, S., Honerkamp-Smith, A. R., Haas, P. A., Trong, P. K. & Goldstein, R. E. Dynamics of a Volvox embryo turning itself inside out. *Physical review letters* **114**, 178101 (2015).

16 Bi, D., Yang, X., Marchetti, M. C. & Manning, M. L. Motility-driven glass and jamming transitions in biological tissues. *Physical Review X* **6**, 021011 (2016).

17 Delarue, M. *et al.* Self-driven jamming in growing microbial populations. *Nature physics* **12**, 762-766 (2016).

18 Jacobeen, S. *et al.* Cellular packing, mechanical stress and the evolution of multicellularity. *Nature physics* **14**, 286-290 (2018).

19 Boraas, M. E., Seale, D. B. & Boxhorn, J. E. Phagotrophy by a flagellate selects for colonial prey: a possible origin of multicellularity. *Evolutionary Ecology* **12**, 153-164 (1998).

20 H. Koschwanez, J., R. Foster, K. & W. Murray, A. Sucrose utilization in budding yeast as a model for the origin of undifferentiated multicellularity. *PLoS biology* **9**, e1001122 (2011).

21 Ratcliff, W. C., Denison, R. F., Borrello, M. & Travisano, M. Experimental evolution of multicellularity. *Proceedings of the National Academy of Sciences* **109**, 1595-1600 (2012).

22 Ratcliff, W. C. *et al.* Experimental evolution of an alternating uni-and multicellular life cycle in Chlamydomonas reinhardtii. *Nature communications* **4**, 1-7 (2013).

23 Herron, M. D. *et al.* De novo origins of multicellularity in response to predation. *Scientific reports* **9**, 1-9 (2019).
24 Westbrook, J. W. *et al.* What makes a leaf tough? Patterns of correlated evolution between leaf toughness traits and demographic rates among 197 shade-tolerant woody species in a neotropical forest. *The American Naturalist* **177**, 800-811 (2011).
25 Veres, S. P. & Lee, J. M. Designed to fail: a novel mode of collagen fibril disruption and its relevance to tissue toughness. *Biophysical journal* **102**, 2876-2884 (2012).
26 Prakash, V. N., Bull, M. S. & Prakash, M. Motility-induced fracture reveals a ductile-to-brittle crossover in a simple animal's epithelia. *Nature Physics* **17**, 504-511 (2021).
27 Grant, N. A., Maddamsetti, R. & Lenski, R. E. Maintenance of metabolic plasticity despite relaxed selection in a long-term evolution experiment with Escherichia coli. *The American Naturalist* **198**, 93-112 (2021).
28 Ratcliff, W. C., Fankhauser, J. D., Rogers, D. W., Greig, D. & Travisano, M. Origins of multicellular evolvability in snowflake yeast. *Nature communications* **6**, 1-9 (2015).
29 Heinrich, E. C., Farzin, M., Klok, C. J. & Harrison, J. F. The effect of developmental stage on the sensitivity of cell and body size to hypoxia in Drosophila melanogaster. *Journal of Experimental Biology* **214**, 1419-1427 (2011).
30 Lenski, R. E., Rose, M. R., Simpson, S. C. & Tadler, S. C. Long-term experimental evolution in Escherichia coli. I. Adaptation and divergence during 2,000 generations. *The American Naturalist* **138**, 1315-1341 (1991).
31 Jacobeen, S. *et al.* Geometry, packing, and evolutionary paths to increased multicellular size. *Physical Review E* **97**, 050401 (2018).
32 Pentz, J. T. *et al.* Ecological advantages and evolutionary limitations of aggregative multicellular development. *Current Biology* **30**, 4155-4164. e4156 (2020).
33 Denk, W. & Horstmann, H. Serial block-face scanning electron microscopy to reconstruct three-dimensional tissue nanostructure. *PLoS Biol* **2**, e329 (2004).
34 Edwards, C. E., Mai, D. J., Tang, S. & Olsen, B. D. Molecular anisotropy and rearrangement as mechanisms of toughness and extensibility in entangled physical gels. *Physical Review Materials* **4**, 015602 (2020).
35 Brown, E., Nasto, A., Athanassiadis, A. G. & Jaeger, H. M. Strain stiffening in random packings of entangled granular chains. *Physical review letters* **108**, 108302 (2012).
36 Raymer, D. M. & Smith, D. E. Spontaneous knotting of an agitated string. *Proceedings of the National Academy of Sciences* **104**, 16432-16437 (2007).
37 Wilhelm, J. & Frey, E. Elasticity of stiff polymer networks. *Physical review letters* **91**, 108103 (2003).
38 Kim, J., Zhang, G., Shi, M. & Suo, Z. Fracture, fatigue, and friction of polymers in which entanglements greatly outnumber cross-links. *Science* **374**, 212-216 (2021).
39 Tauber, J., Rovigatti, L., Dussi, S. & Van Der Gucht, J. Sharing the load: Stress redistribution governs fracture of polymer double networks. *Macromolecules* **54**, 8563-8574 (2021).
40 Sheu, Y.-J., Barral, Y. & Snyder, M. Polarized growth controls cell shape and bipolar bud site selection in Saccharomyces cerevisiae. *Molecular and cellular biology* **20**, 5235-5247 (2000).
41 Watanabe, M., Watanabe, D., Nogami, S., Morishita, S. & Ohya, Y. Comprehensive and quantitative analysis of yeast deletion mutants defective in apical and isotropic bud growth. *Current genetics* **55**, 365-380 (2009).
42 Sopko, R. *et al.* Mapping pathways and phenotypes by systematic gene overexpression. *Molecular cell* **21**, 319-330 (2006).
43 Lee, D. H., Tamura, A., Arisaka, Y., Seo, J.-H. & Yui, N. Mechanically reinforced gelatin hydrogels by introducing slidable supramolecular cross-linkers. *Polymers* **11**, 1787 (2019).

44 Gerhards, C. *Effects of type of testing equipment and specimen size on toughness of wood*. Vol. 97 (Forest Products Laboratory, 1968).
45 Okasha, S. Multilevel selection and the major transitions in evolution. *Philosophy of science* **72**, 1013-1025 (2005).
46 Rainey, P. B. & Kerr, B. Cheats as first propagules: a new hypothesis for the evolution of individuality during the transition from single cells to multicellularity. *BioEssays* **32**, 872-880 (2010).
47 Graessley, W. W. in *The entanglement concept in polymer rheology* 1-179 (Springer, 1974).
48 Chen, W., Yu, H., Li, Q., Liu, Y. & Li, J. Ultralight and highly flexible aerogels with long cellulose I nanofibers. *Soft matter* **7**, 10360-10368 (2011).
49 Gravish, N., Franklin, S. V., Hu, D. L. & Goldman, D. I. Entangled granular media. *Physical review letters* **108**, 208001 (2012).
50 Zou, L.-N., Cheng, X., Rivers, M. L., Jaeger, H. M. & Nagel, S. R. The packing of granular polymer chains. *Science* **326**, 408-410 (2009).
51 Savoie, W., Tuazon, H., Bhamla, M. S. & Goldman, D. I. Amorphous Entangled Active Matter. *arXiv preprint arXiv:2207.03665* (2022).
52 Ozkan-Aydin, Y., Goldman, D. I. & Bhamla, M. S. Collective dynamics in entangled worm and robot blobs. *Proceedings of the National Academy of Sciences* **118**, e2010542118 (2021).
53 Patil, V. P. *et al.* Ultrafast reversible self-assembly of living tangled matter. *arXiv preprint arXiv:2210.03384* (2022).
54 Nagy, L. G. in *The Evolution of Multicellularity* 279-300 (CRC Press, 2022).
55 Moore, D. *Fungal biology in the origin and emergence of life*. (Cambridge University Press, 2013).
56 García-Segovia, P., Andrés-Bello, A. & Martínez-Monzó, J. Rehydration of air-dried Shiitake mushroom (Lentinus edodes) caps: Comparison of conventional and vacuum water immersion processes. *LWT-Food Science and Technology* **44**, 480-488 (2011).
57 Roth, R., Wagner, R. & Goodenough, U. Lichen 3. Outer layers. *Algal Research* **56**, 102332 (2021).
58 Yanni, D. *et al.* Topological constraints in early multicellularity favor reproductive division of labor. *Elife* **9**, e54348 (2020).
59 Larson, B. T. *et al.* Biophysical principles of choanoflagellate self-organization. *Proceedings of the National Academy of Sciences* **117**, 1303-1311 (2020).
60 Brunet, T. *et al.* Light-regulated collective contractility in a multicellular choanoflagellate. *Science* **366**, 326-334 (2019).
61 Dayel, M. J. *et al.* Cell differentiation and morphogenesis in the colony-forming choanoflagellate Salpingoeca rosetta. *Developmental biology* **357**, 73-82 (2011).
62 Hinkle, P. C., Kumar, M. A., Resetar, A. & Harris, D. L. Mechanistic stoichiometry of mitochondrial oxidative phosphorylation. *Biochemistry* **30**, 3576-3582 (1991).
63 Raymond, J. & Segrè, D. The effect of oxygen on biochemical networks and the evolution of complex life. *Science* **311**, 1764-1767 (2006).
64 Szathmáry, E. & Smith, J. M. The major evolutionary transitions. *Nature* **374**, 227-232 (1995).
65 Buss, L. W. *The evolution of individuality*. Vol. 796 (Princeton University Press, 2014).
66 Lewontin, R. C. The units of selection. *Annual review of ecology and systematics*, 1-18 (1970).
67 Michod, R. E. in *The Evolution of Multicellularity* 25-52 (CRC Press, 2022).
68 Libby, E. & Rainey, P. B. A conceptual framework for the evolutionary origins of multicellularity. *Physical biology* **10**, 035001 (2013).

69 Tong, K., Bozdag, G. O. & Ratcliff, W. C. Selective drivers of simple multicellularity. *Current Opinion in Microbiology* **67**, 102141 (2022).
70 Gietz, R. D. & Schiestl, R. H. High-efficiency yeast transformation using the LiAc/SS carrier DNA/PEG method. *Nature protocols* **2**, 31-34 (2007).
71 Deerinck, T. J. *et al.* High-performance serial block-face SEM of nonconductive biological samples enabled by focal gas injection-based charge compensation. *Journal of microscopy* **270**, 142-149 (2018).
72 Ngo, H. T. & Yin, C. S. Luteimonas terrae sp. nov., isolated from rhizosphere soil of Radix ophiopogonis. *International journal of systematic and evolutionary microbiology* **66**, 1920-1925 (2016).
73 Zamani-Dahaj, S. A. *et al.* Spontaneous emergence of multicellular heritability. *bioRxiv* (2021).
74 Li, H. Aligning sequence reads, clone sequences and assembly contigs with BWA-MEM. *arXiv preprint arXiv:1303.3997* (2013).
75 McKenna, A. *et al.* The Genome Analysis Toolkit: a MapReduce framework for analyzing next-generation DNA sequencing data. *Genome research* **20**, 1297-1303 (2010).
76 Garrison, E. & Marth, G. Haplotype-based variant detection from short-read sequencing. *arXiv preprint arXiv:1207.3907* (2012).
77 Danecek, P. *et al.* The variant call format and VCFtools. *Bioinformatics* **27**, 2156-2158 (2011).
78 Thorvaldsdóttir, H., Robinson, J. T. & Mesirov, J. P. Integrative Genomics Viewer (IGV): high-performance genomics data visualization and exploration. *Briefings in bioinformatics* **14**, 178-192 (2013).
79 Danecek, P. *et al.* Twelve years of SAMtools and BCFtools. *Gigascience* **10**, giab008 (2021).
80 Cingolani, P. *et al.* A program for annotating and predicting the effects of single nucleotide polymorphisms, SnpEff: SNPs in the genome of Drosophila melanogaster strain w1118; iso-2; iso-3. *Fly* **6**, 80-92 (2012).
81 Cherry, J. M. *et al.* Saccharomyces Genome Database: the genomics resource of budding yeast. *Nucleic acids research* **40**, D700-D705 (2012).
82 Day, T. C. *et al.* Cellular organization in lab-evolved and extant multicellular species obeys a maximum entropy law. *Elife* **11**, e72707 (2022).

Acknowledgements. We thank Jennifer T. Pentz for teaching us Illumina library preparation, Shweta Biliya at the High Throughput DNA Sequencing Core at Georgia Tech for sequencing the genomes of evolved strains, and Kingsley A. Boateng at Core Facilities at the Carl R. Woese Institute for Genomic Biology for the SEM imaging. Siyi Cao helped us with microscopy during the early stages of this project. We thank Christian Orlic, László Nagy, and all members of the Ratcliff group for insightful comments on the manuscript. This work was supported by NIH grants R35-GM138030-01 to W.C.R. and R35-GM138354-02 to P.J.Y., and a Packard Fellowship for Science and Engineering to W.C.R.

Author Contributions. G.O.B., A.Z., P.J.Y, and W.C.R. conceived of the project. G.O.B. and W.C.R. designed the MuLTEE, and G.O.B. performed the evolution experiment. G.O.B., A.Z., P.K., and T.C.D. designed and collected data. A.Z. generated SBF-SEM images. A.Z., T.C.D., and P.J.Y performed the yeast biophysical simulations. E.L.D. and A.H.B. assisted G.O.B. and A.Z. with image analysis. A.J.B. genetically engineered large snowflake yeast, K.T. performed life-cycle experiments, D.T.L. measured the number of generations, and P.L.C. performed unicellular reversion experiments. G.O.B., A.Z., T.C.D., W.C.R., and P.Y. analyzed the data. G.O.B. made the figures. G.O.B., W.C.R., and P.J.Y. wrote the first draft of the paper, and all authors contributed to the revision.

Competing interests. The authors have no competing interests to declare.

Data and code availability. All source data and code are available at https://github.com/ozanbozdag/de_novo_evolution_of_macroscopic_multicellularity. Microscopy images are available upon request.

Extended Data Figures

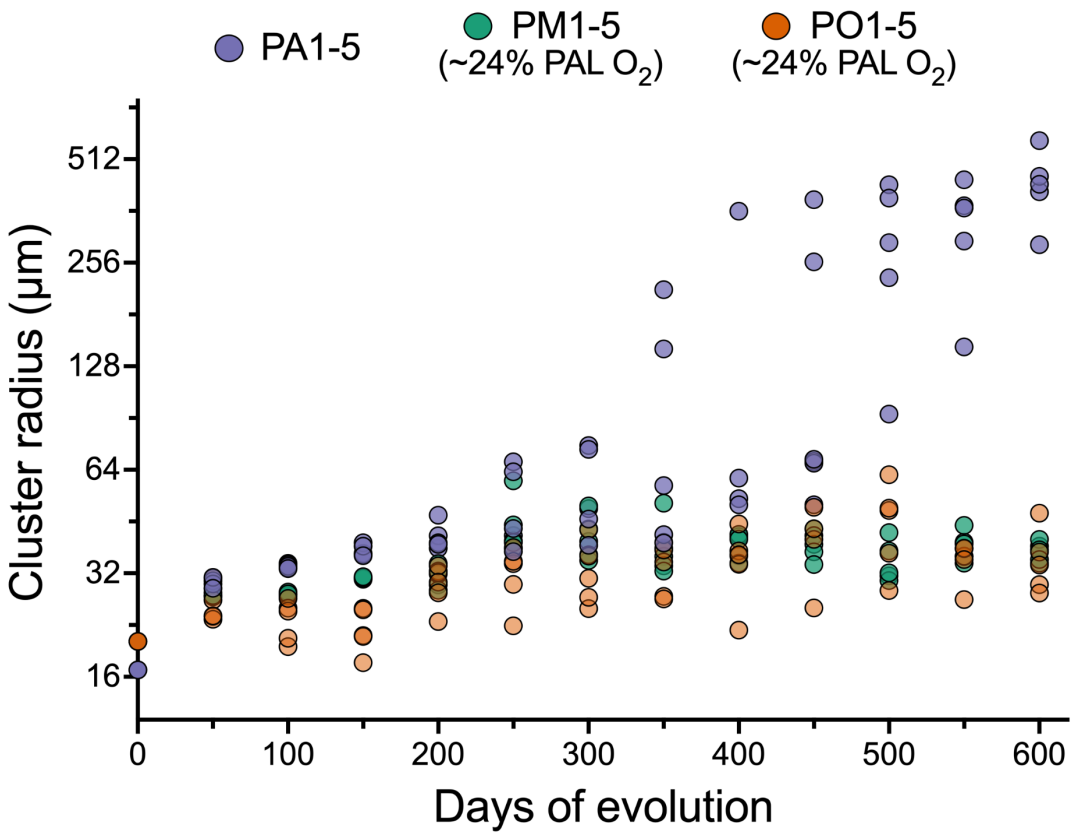

Extended Data Figure 1. Temporal dynamics of size evolution in each population and treatment group. Data points show the weighted average radius of cluster size for the whole population (see Methods for details).

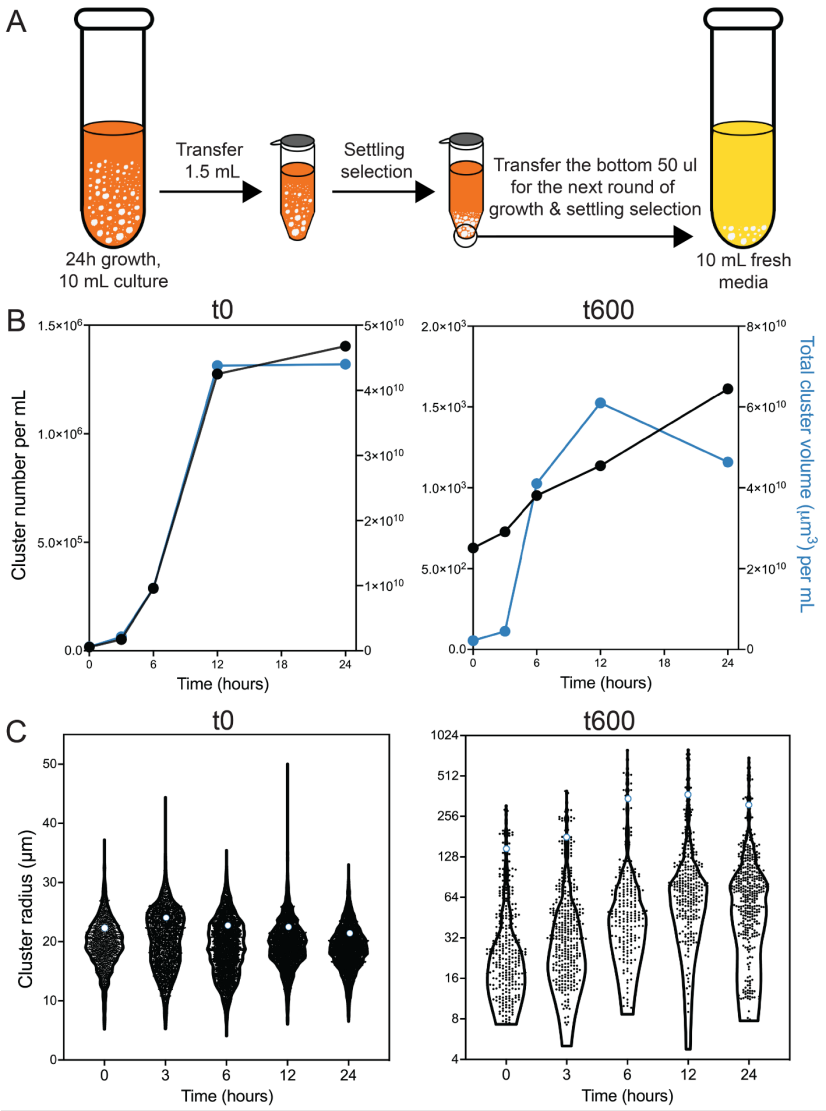

Extended Data Figure 2. Characterizing the life-cycle of the ancestral (microscopic) and evolved (macroscopic) snowflake yeast. A) During the ~24-hour growth cycle, snowflake yeast compete for growth and reproduction in 10 mL of YPED (250 RPM at 30°C). At the end of the growth phase, we select for larger group size via settling selection. While there is a theoretical maximum survival rate of 15% (that is, if all of the cells survived settling selection), we only transfer the bottom 50 µl of pellet biomass regardless of how many cells settle, creating an arms race that favors the fastest groups within the population. Our measurements of the number of cellular generations per day in Figure 1A suggests about 3%

878 of the cells survive from one day to the next on average. B) Both the microscopic (ancestral)
879 and macroscopic (t600) snowflake yeast clusters have a life cycle, reproducing during the
880 growth phase. C) Consistent with entanglement producing tough groups, macroscopic
881 snowflake yeast release mostly microscopic propagules, possibly from branch tips at the
882 exterior of the group, where the opportunity for entanglement is minimal. Despite the
883 presence of many small propagules, most of the biomass in the population is contained
884 within macroscopic clusters. The open circles represent the biomass-weighted mean size,
885 which is the average sized group the mean cell finds itself in.

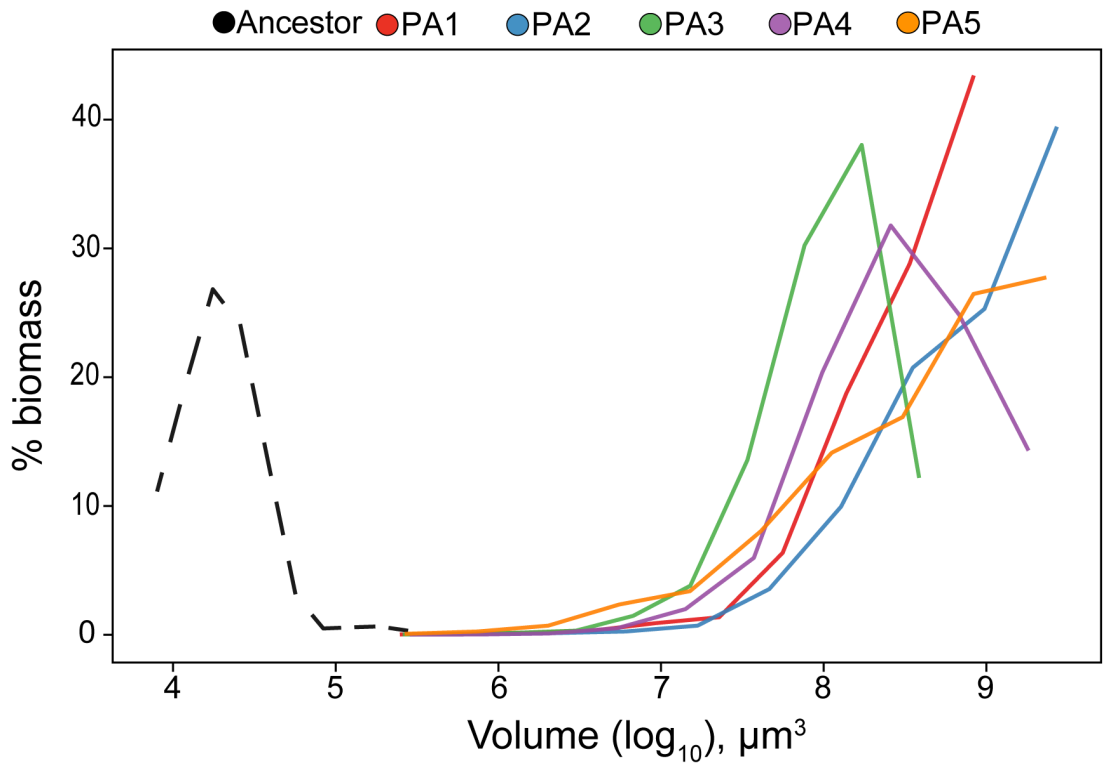

Extended Data Figure 3. Biomass distribution as a function of group size for the ancestral snowflake yeast (dotted line) and 600 day evolved populations of PA1-PA5. The 'weighted mean size' used in Figures 1, 2 and 4 is the mean of the biomass distribution.

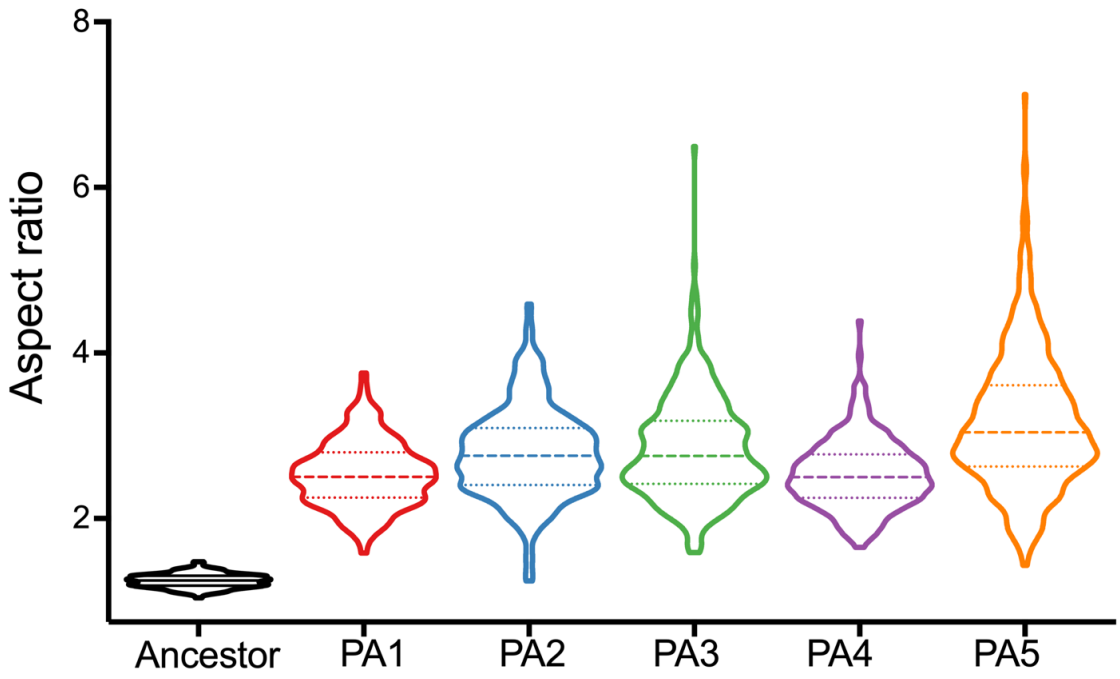

890

891 **Extended Data Figure 4.** Distribution of aspect ratios for ancestral and 600-day evolved

892 populations of anaerobic snowflake yeast.

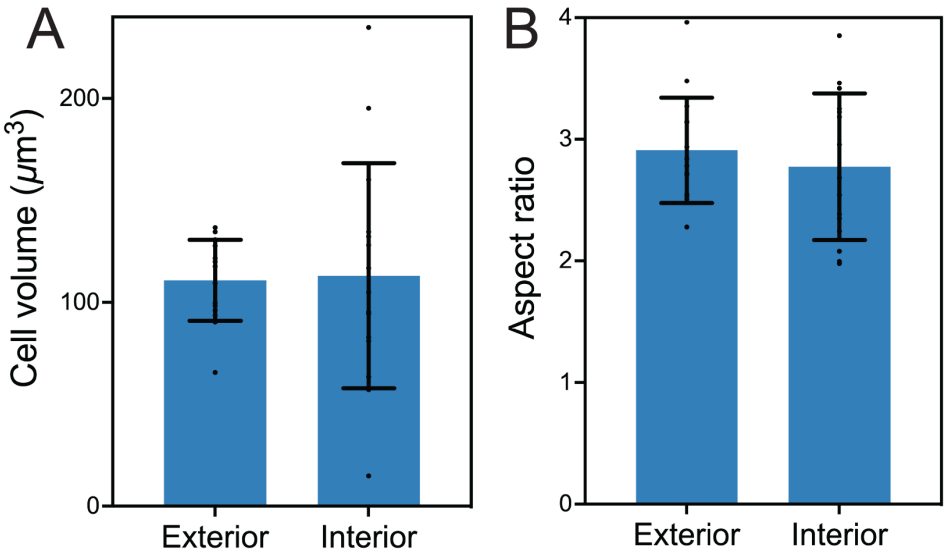

Extended Data Figure 5. Cell shape is not substantially affected by location within macroscopic yeast. (A) and (B) show cell volume and cell shape (aspect ratio) measured for 10 cells from the interior of a macroscopic cluster and 10 cells from the exterior of a cluster (measured in t600 macroscopic clusters). Average cell volume for exterior and interior are 110.8 μm^3 and 113.1 μm^3 (p=0.88, t=0.15 df=17.55, Welch's t-test), and average cell shape for exterior and interior are 2.9 and 2.8 (p=0.51, t=0.68, df=14, Welch's t-test). Individual measurements are marked as points, the mean and one standard deviation are indicated by the bar plot.

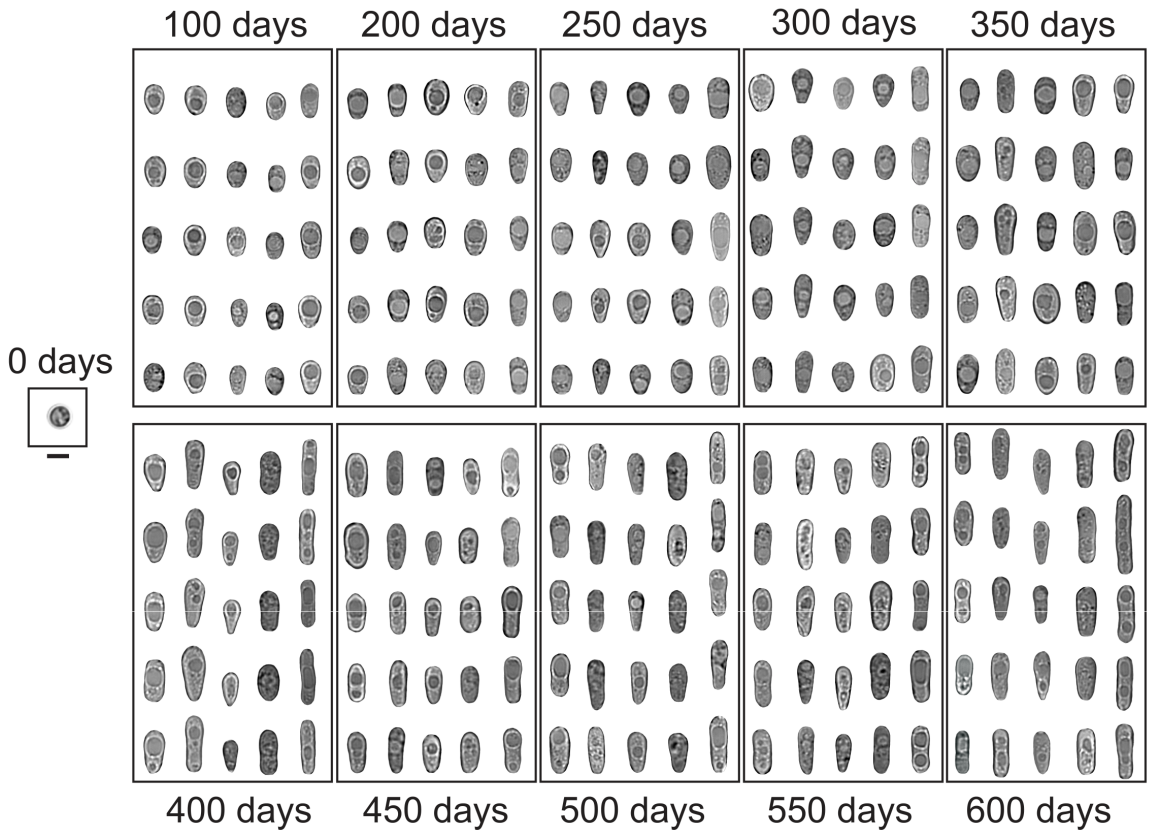

Extended Data Figure 6. Parallel evolution of elongated cell shape across all five replicates of each PA population. For each evolutionary time point and population, five different cells are shown (organized vertically from left to right: PA1 on the further left and PA5 on the further right in each box). Scale bar is 5 μm (under the ancestral cell). This is a more detailed version of the plot shown in Figure 2c.

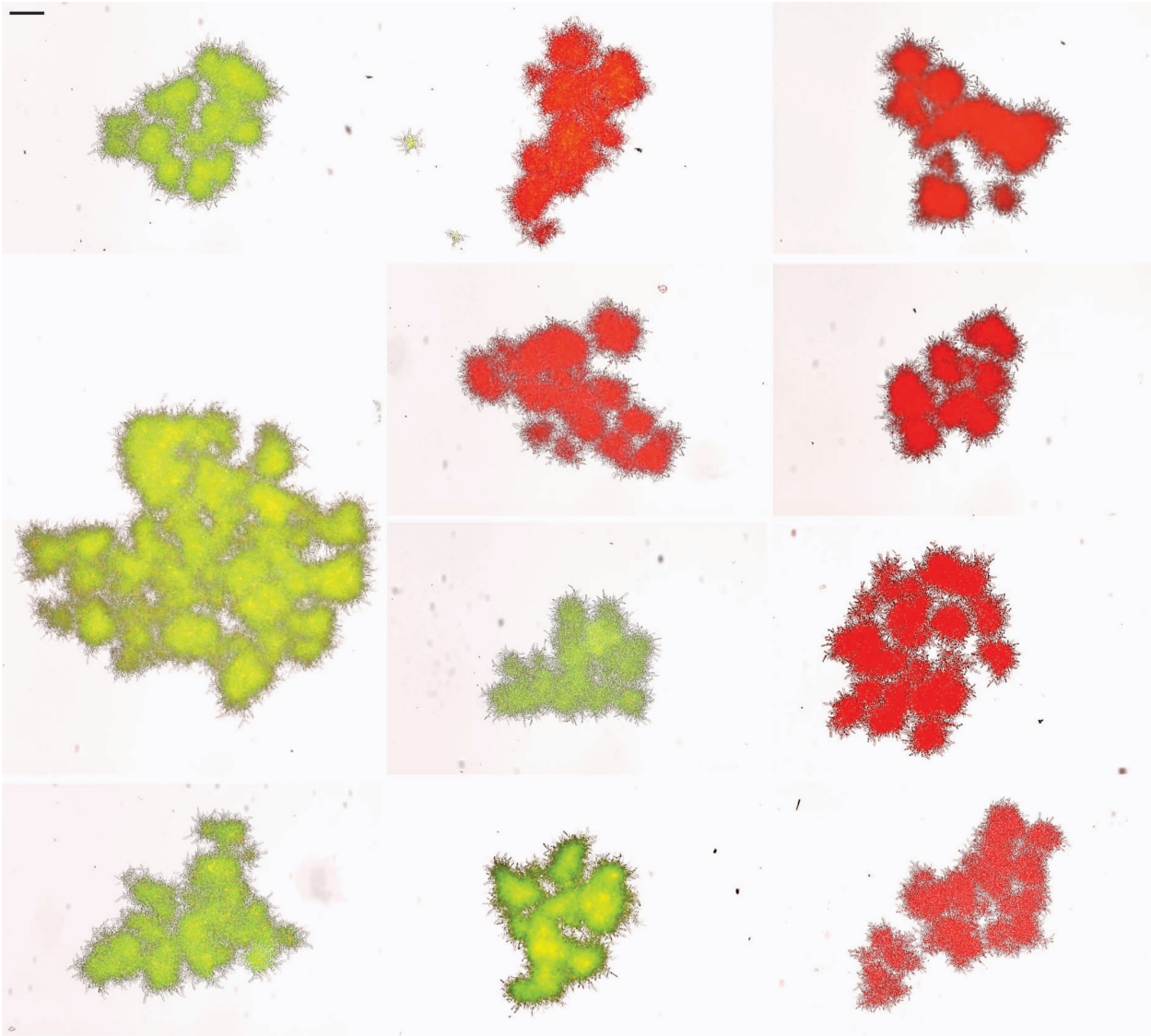

907

908 **Extended Data Figure 7.** Macroscopic snowflake yeast are monoclonal, growing via permanent
909 mother-daughter cellular bonds, not aggregation. We co-cultured GFP and RFP-tagged genotypes
910 of a macroscopic single strain isolate (PA2, strain ID: GOB1413-600) for 5 days, then imaged 70
911 clusters on a Nikon Ti-E. Shown are a composite of 11 individual clusters, which all remain
912 entirely green or red. Individual clusters were compressed with a coverslip for imaging, resulting
913 in their fragmentation into multiple modules. Scale bar (top-left) is 100 μm.

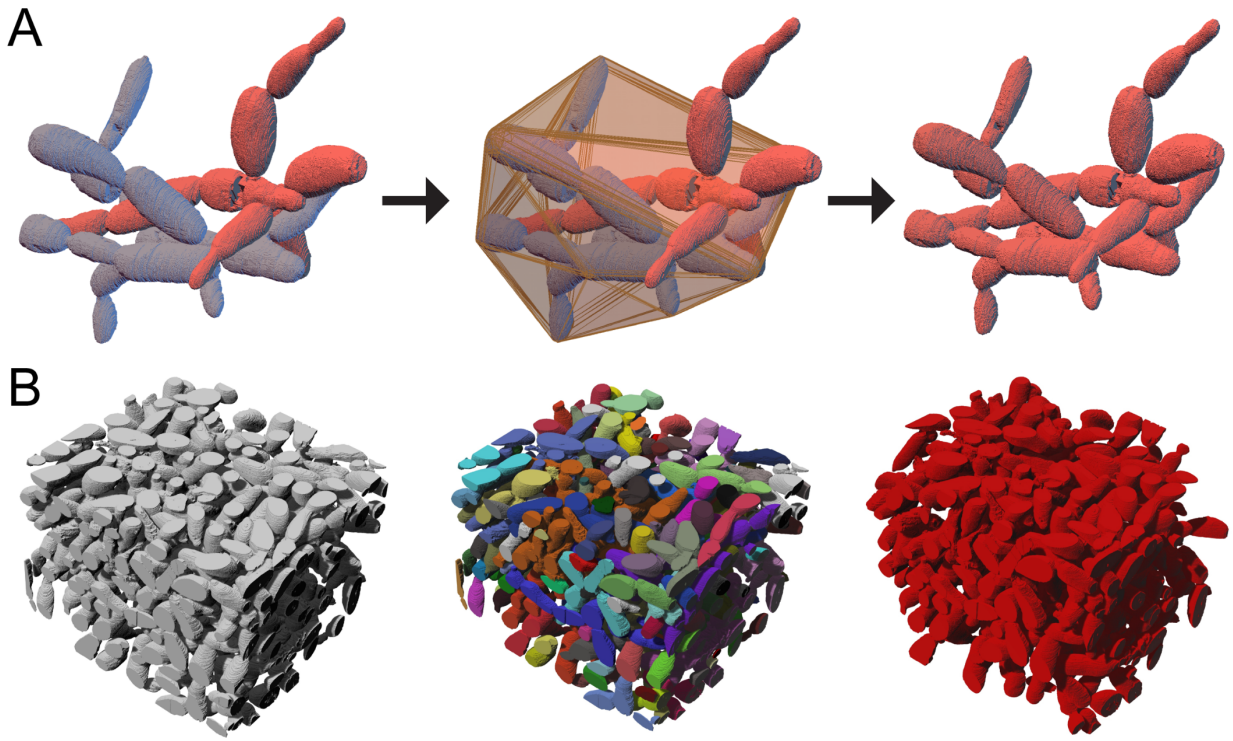

Extended Data Figure 8. Quantifying entanglement via analysis of the topology and geometry of a snowflake yeast cluster. (A) We measured entanglement of individual components by fitting a convex hull around each component, and determining whether the other component overlaps with the space bounded by this convex hull. Here we just show the convex hull for the blue component, which overlaps with the red component. These components are thus part of the same entangled component. (B) Using this approach, we identified the components within a sub-volume of a macroscopic snowflake yeast, and used a percolation analysis to examine the fraction of the biomass that is part of the same entangled component (colored in red).

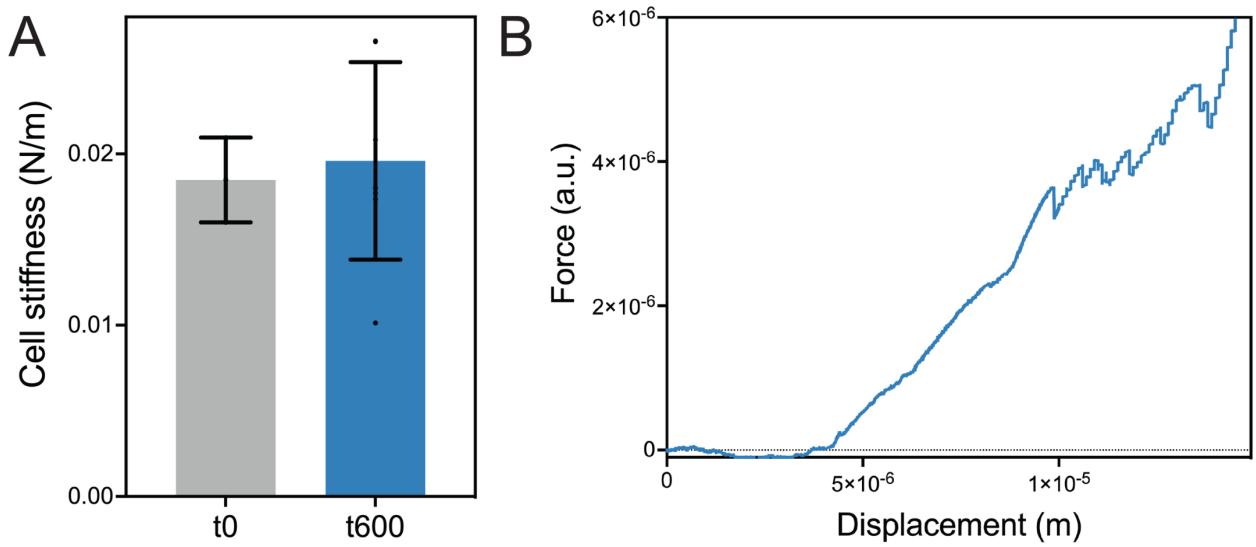

Extended Data Figure 9. (A) Individual cells do not change their stiffness over 600 rounds of selection (average cell stiffness for the ancestor and t600 isolates are 0.019 and 0.020, respectively. p=0.77, t=0.31, df=8, Welch's unequal variances t-test). Single-cell stiffness values measured from atomic force microscopy (AFM) of individual cells. Error bars are one standard deviation. (B) Macroscopic snowflake yeast fractured into small modules prior to compression do not show strain stiffening behavior. Shown here is an AFM trajectory of cantilever deflection vs displacement for one t600 cluster that has been crushed into small, unentangled pieces.

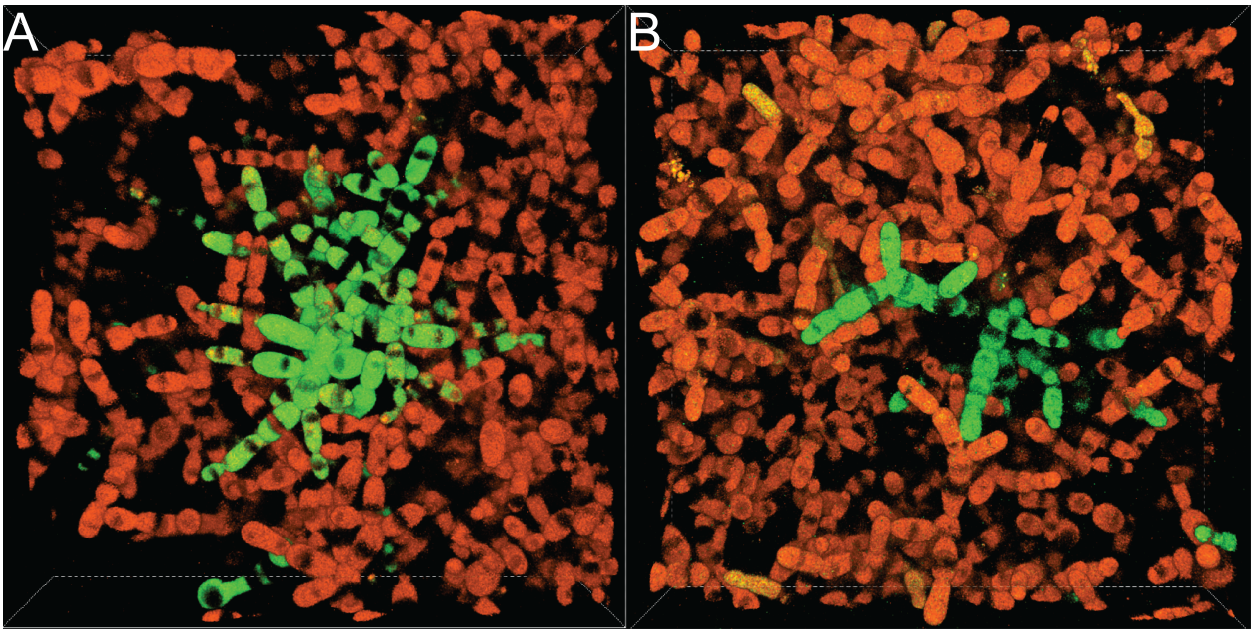

Extended Data Figure 10. Representative confocal images show chimeric clusters that are formed after growth in liquid culture followed by entanglement on agar plates. Each frame is 139.64 x 139.64 x 34.50 µm in X, Y, and Z axes, respectively.

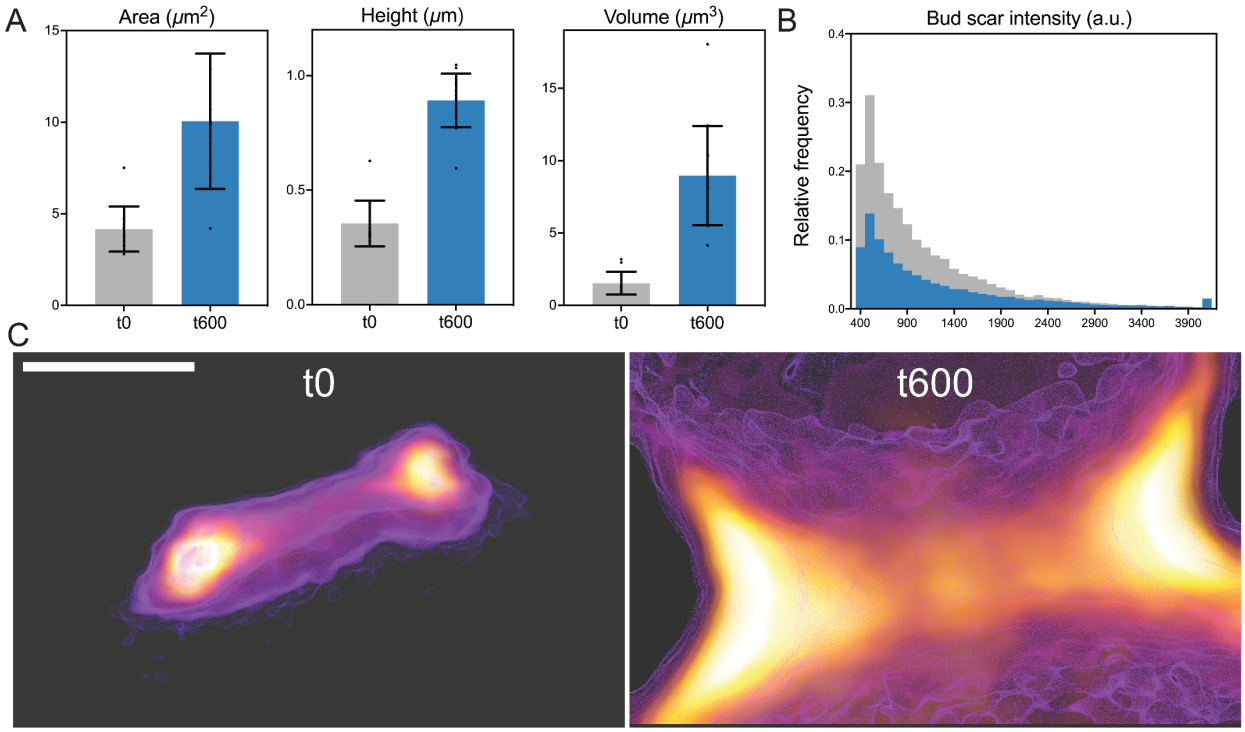

936

937 **Extended Data Figure 11.** Dimensions of bud scars connecting cells in microscopic, ancestral
938 (t0, gray) and macroscopic, evolved snowflake yeast clusters (PA2 t600, blue). Macroscopic t600
939 yeast had 2.4x larger bud scar cross-sectional area (A; t=5.3, df=24, p<0.001), 2.8x greater bud
940 scar height (B; t=12.5, df=24, p<0.001), resulting in bud scars with 5.8-fold greater volume (C;
941 t=7.3, df=24, p<0.001) than the microscopic ancestor. Error bars are one standard deviation. (B)
942 Histogram of pixel intensities for bud scars stained with chitin stain calcofluor white, isolated from
943 ancestor (t0, microscopic) and t600 (macroscopic) bud scars. The t600 strain has a 27% higher
944 mean fluorescence intensity, suggesting that they may have evolved moderately chitin density in
945 the bud scar. (C) The size differences in bud scars is readily visible. Shown are the side view of
946 buds from the ancestor (left) and t600 evolved (right), imaged at the same microscope settings.
947 The scale bar is 0.5 µm.

948 **Supplementary Movie 1.** Comparison of the ancestor and a population of macroscopic snowflake
949 yeast (PA2-t600, on the right).
950
951 **Supplementary Table 1.** A list of primers, plasmids, and strains used in the study.
952
953 **Supplementary File 1.** Code for the simple 3D biophysical simulation. These simulations,
954 described at a high level in the methods section of this paper, were adapted from previous work by
955 Jacobeen 2018 and Day 2022 [31,82]. The code is self-contained and commented. Please reach out to
956 Thomas Day or Peter Yunker with questions.